

# The gradient of diffuse $\gamma$ -ray emission in the Galaxy

D. Breitschwerdt<sup>1</sup>, V. A. Dogiel<sup>2,3</sup>, and H. J. Völk<sup>4</sup>

<sup>1</sup> Max-Planck Institut für extraterrestrische Physik, Postfach 1312, 85741 Garching, Germany  
e-mail: breitsch@mpe.mpg.de

<sup>2</sup> P.N.Lebedev Physical Institute, 119991 Moscow GSP-1, Russia  
e-mail: dogiel@lpi.ru

<sup>3</sup> Institute of Space and Astronautical Science, 3-1-1 Yoshinodai, Sagamihara, Kanagawa 229-8510, Japan  
e-mail: vad@astro.isas.ac.jp

<sup>4</sup> Max-Planck Institut für Kernphysik, Postfach 103 980, 69029 Heidelberg, Germany  
e-mail: Heinrich.Voelk@mpi-hd.mpg.de

Received 12 June 2001 / Accepted 16 January 2002

**Abstract.** We show that the well-known discrepancy, known for about two decades, between the radial dependence of the Galactic cosmic ray nucleon distribution, as inferred most recently from EGRET observations of diffuse  $\gamma$ -rays above 100 MeV, and of the most likely cosmic ray source distribution (supernova remnants, superbubbles, pulsars) can be explained purely by *propagation* effects. Contrary to previous claims, we demonstrate that this is possible, if the dynamical coupling between the escaping cosmic rays and the thermal plasma is taken into account, and thus a self-consistent calculation of a *Galactic Wind* is carried out. Given a dependence of the cosmic ray source distribution on Galactocentric radius  $r$ , our numerical wind solutions show that the cosmic ray outflow velocity,  $V(r, z) = u_0 + V_{A0}$ , also depends both on  $r$ , as well as on vertical distance  $z$ , with  $u_0$  and  $V_{A0}$  denoting the thermal gas and the Alfvén velocities, respectively, at a reference level  $z_C$ . The latter is by definition the transition boundary from diffusion to advection dominated cosmic ray transport and is therefore also a function of  $r$ . In fact, the cosmic ray escape time averaged over particle energies decreases with increasing cosmic ray source strength. Thus an increase in cosmic ray source strength is counteracted by a reduced average cosmic ray residence time in the gas disk. This means that pronounced peaks in the radial distribution of the source strength result in mild radial  $\gamma$ -ray gradients at GeV energies, as it has been observed. The effect might be enhanced by anisotropic diffusion, assuming different radial and vertical diffusion coefficients. In order to better understand the mechanism described, we have calculated analytic solutions of the stationary diffusion-advection equation, including anisotropic diffusion in an axisymmetric geometry, for a given cosmic ray source distribution and a realistic outflow velocity field  $V(r, z)$ , as inferred from the self-consistent numerical Galactic Wind simulations performed simultaneously. At TeV energies the  $\gamma$ -rays from the sources themselves are expected to dominate the observed “diffuse” flux from the disk. Its observation should therefore allow an empirical test of the theory presented.

**Key words.** cosmic rays – MHD – gamma rays: observations – ISM: supernova remnants

## 1. Introduction

Our information on the spatial distribution of cosmic rays (CRs) in the Galaxy stems largely from measurements of nonthermal emission, generated by the energetic charged particles interacting with matter and electromagnetic fields. For  $\gamma$ -ray energies above 100 MeV, the main production process is probably via  $\pi^0$ -decay, resulting from nuclear collisions between high energy particles and interstellar matter. Past and recent observations in the GeV range have shown a roughly uniform distribution of diffuse  $\gamma$ -ray emissivity in the Galactic plane,

exhibiting only a shallow radial gradient (in a cylindrical Coordinate system). Hence, if  $\gamma$ -rays were to map the spatial CR distribution, we would expect it to be uniform as well. However, associating CR production regions with star formation regions, all possible Galactic CR *source* distributions are strongly peaked towards a Galactocentric distance at which a ring of molecular gas resides. It is commonly believed that the bulk of the CR nucleons below about  $10^{15}$  eV is produced in supernova remnants (SNRs) – the majority being core collapse SNRs – most likely by diffusive shock acceleration (Krymsky 1977; Axford et al. 1977; Bell 1978a,b; Blandford & Ostriker 1978). It has been argued that up to some tenths of the hydrodynamic explosion energy might be converted into CR

---

Send offprint requests to: D. Breitschwerdt,  
e-mail: breitsch@mpe.mpg.de

energy (e.g., Berezhko et al. 1994). Since high-mass star formation mostly occurs in a spatially nonuniform manner, i.e. in OB associations predominantly located in the spiral arms of late type galaxies, we are confronted with the problem of reproducing a mild radial gradient in the diffuse Galactic  $\gamma$ -ray emission as it has been observed for the first time by the COS-B satellite (Strong et al. 1988) and, more recently, with higher angular and energy resolution, higher sensitivity and lower background by the EGRET instrument of the CGRO satellite (Strong & Mattox 1996; Digel et al. 1996). If the SNRs are the sources of the CR nucleon component and if the source distribution is inhomogeneous, this discrepancy must arise during the *propagation* of CRs from their sources through the interstellar medium. Unlike e.g. the interpretation of radio synchrotron emission, generated by relativistic electrons,  $\gamma$ -ray data open the possibility of studying the nucleonic component of the CRs, in which almost all of the energy is stored (see e.g., Dogiel & Schönfelder 1997). The distribution of the  $\gamma$ -ray emissivity in the Galactic disk therefore bears important information on the origin of CRs and on the conditions of CR propagation in the Galaxy.

## 2. Gradient of the $\gamma$ -ray emissivity in the galactic disk

The first data on the radial distribution (i.e. gradient) of the  $\gamma$ -ray emissivity in the disk were obtained with the SAS-II satellite (energy range 30–200 MeV). The data showed rather strong variations of the emissivity along the Galactic plane which dropped rapidly with radius (see e.g., Stecker & Jones 1977), in rough agreement with the distribution of candidate CR sources in the Galaxy such as SNRs or pulsars. A noticeable discrepancy however emerged from the COS-B data (energy range 70–5000 MeV), in which the emissivity gradient was found to be rather small, when compared to the SNR distribution, especially at high energies ( $E_\gamma > 300$  MeV), with a maximum variation by a factor of only 2 (see Strong et al. 1988). An energy dependence of the gradient was mentioned by almost all groups analyzing the COS-B data and was usually interpreted as a steeper gradient for CR electrons, producing the soft part of the  $\gamma$ -ray spectrum, compared to nuclei. Detailed analyses of different models of CR propagation based on the gradient value were usually performed with the COS-B data because of their much better statistics compared with the SAS-II data.

The recent measurements with the EGRET instrument onboard CGRO, obtained by different methods at energies 100–10000 MeV, showed that the emissivity drops at the edge of the disk. Digel et al. (1996), performed a study of the outer part of the Galaxy towards molecular complexes, the Cepheus and Polaris Flares in the local arm and the larger molecular complex in the Perseus arm. Since the total masses of these complexes are known, it was possible to infer the CR density from the measured  $\gamma$ -ray fluxes in the direction of these objects.

It was discovered that the apparent emissivity decreases by a factor 1.7, which is somewhat smaller than that for COS-B. The analysis of Strong & Mattox (1996), based on a model of the average gas density distribution in the disk, shows a smaller intensity gradient which does not differ significantly from that of COS-B in the Galactic disk.

One of the important conclusions which follows from all these data, and which we will discuss below, is that the distribution of the  $\gamma$ -emissivity in the disk in the GeV range is rather uniform compared with the most probable distribution of CR sources.

## 3. Basic ideas for a new approach of CR propagation in the galaxy

A natural explanation of a uniform CR distribution would be effective radial mixing due to the diffusion of CRs produced in different parts of the Galactic disk. It is then straightforward to infer the mixing volume, which usually includes the Galactic disk plus a large Galactic halo; the details of such a model were discussed in the book of Ginzburg & Syrovatskii (1964). This 3-dimensional cylindrical model, which includes diffusive-advective transport, a free escape of cosmic rays from the halo boundary into intergalactic space, and the observed supernova shells as sources of cosmic rays in the Galactic disk, explained very well characteristics of the Galactic radio and  $\gamma$ -ray emission as well as the data on cosmic ray spectra and their chemical composition including stable and radioactive secondary nuclei, intensities of positrons and antiprotons etc. (a summary of this analysis can be found in Berezhinskii et al. 1990).

In general the propagation equation for CRs is described by

$$-\nabla_i(D_{ij}\nabla_j n - U_i n) + \frac{\partial}{\partial E} \left( \frac{dE}{dt} n \right) = Q(r, E), \quad (1)$$

where  $D_{ij}$  is the diffusion tensor and  $U_i$  is the advection velocity, which in general are functions of the coordinates, and  $dE/dt$  is the term which describes particle energy losses including adiabatic losses if the velocities vary spatially. The right hand side of the equation describes the spatial and energy dependence of the source density, derived from radio observations of the SNR distribution and the injection spectrum of CRs.

The main conclusion was that almost all observations can be reasonably explained if the halo extension is about several kpc, the injection spectrum of electrons and protons  $Q(E)$  is a power-law ( $Q(E) \propto E^{-\gamma_0}$  with  $\gamma_0 \simeq 2.2-2.4$ ), and the radially uniform velocity of advection does not exceed the value of  $20 \text{ km s}^{-1}$ . Compton scattering of relativistic electrons was found to play a significant rôle in the halo  $\gamma$ -ray emission. However, this model failed to explain a smooth emissivity distribution of  $\gamma$ -rays in the Galactic disk (see for details Dogiel & Uryson 1988). Even in the case of a very extended halo with a radius larger than 10 kpc the derived emissivity gradient (calculated for

the observed SN distribution) was larger than observed. Only for a hypothetical uniform distribution of the sources in the disk the calculations can reproduce the data.

This model was further developed by Bloemen et al. (1991, 1993). Extensive investigations of the 3-dimensional diffusion-advection transport equation for nucleons, low-energy electrons and the  $\gamma$ -rays showed that even in the most favorable case of an extended halo with a vertical height as large as 20 kpc, their model, although reproducing the COS B data marginally, is not able to remove the signature of the observationally inferred SNR source distribution, i.e. the distribution of the calculated emissivity was still steeper than permitted by the data. The vertical gradient of the advection velocity derived from the fluxes of stable and radioactive nuclei near Earth had to be smaller than  $15 \text{ km s}^{-1}/\text{kpc}$ . The other unexpected conclusion was that the halo extension obtained from the nuclear data was significantly less than estimated from the  $\gamma$ -ray data (see also Webber et al. 1992).

A qualitative argument, how to populate the outer Galaxy with CRs, has been given by Erlykin et al. (1996) who invoke wind removal of particles in the inner Galaxy, combined with some return flow to the outer disk. It is hard to judge the merits of such a suggestion in the absence of any physics estimate. We therefore do not further consider such a possibility here.

Recently, Strong and collaborators in a series of papers (see Strong et al. 2000, and references therein) have developed a numerical method for this model and made a new attempt to analyze the  $\gamma$ -ray emission and the CR data, based on the latest data from COMPTEL, EGRET and OSSE. They limited the analysis to radially uniform diffusion-advection and to diffusion-reacceleration transport models, and concluded that no such diffusion-advection model can adequately describe the data, in particular the B/C ratio and the energy dependence. These authors claimed, however, that by including reacceleration one can account for all the observational data. A peculiar consequence of their analysis was that they did not use the *observed* supernova source distribution (see e.g., Kodeira 1974; Leahy & Xinji 1989; Case & Bhattacharya 1996, 1998) as the *input*  $Q$  for Eq. (1), but rather *derived* it from the  $\gamma$ -ray data to reproduce the observed spatial variations of the emissivity in the disk. The result was a source distribution that is flat in the radial direction.

Thus we see that the conventional model of uniform diffusion-advection has serious problems in spite of its evident achievements. One solution is to assume that some of the observational data are not significant like the SN distribution derived from the radio observations (Strong et al. 2000). The alternative is to conclude that it is time to abandon the standard model, which is what we do in this paper. We shall demonstrate, that strong radial source gradients will be removed by a strong *advection* velocity in the halo (due to a Galactic wind driven by the CRs themselves, see below) that varies with radius  $R$  and height  $z$ . In addition *anisotropic diffusion* with different diffusion coefficients  $D_{\parallel}$  and  $D_{\perp}$  in the disk and the halo,

respectively, might also play a rôle. It should be emphasized that a radially varying advection velocity occurs naturally in spiral galaxies, even for a uniform source distribution, because the gravitational potential increases towards the centre, thus inducing stronger velocity gradients in this direction (see Fig. 2), as has been shown by Breitschwerdt et al. (1991).

The existence of strong advective CR transport in the Galactic halo has been shown on dynamical grounds in a number of papers in the past (Ipavich 1975; Breitschwerdt et al. 1987, 1991, 1993; Fichtner et al. 1991; Zirakashvili et al. 1996; Ptuskin et al. 1997). The key element of halo transport theory is that CRs, which by observations are known to escape from the Galaxy, resonantly generate waves by the so-called streaming instability (Kulsrud & Pearce 1969) leading to strong scattering of CRs. Therefore, even in the case of strong non-linear wave damping, advection is at least as important a CR transport mechanism out to large distances in the halo as diffusion, provided that the level of MHD-turbulence is high enough for coupling between CRs and MHD waves (Dogiel et al. 1994; Ptuskin et al. 1997). There is also growing indirect observational evidence of outflows from the interpretation of soft X-ray data of galactic halos in edge-on galaxies like NGC 4631 (Wang et al. 1995), and also of the soft X-ray background in our own Galaxy (Breitschwerdt & Schmutzler 1994, 1999). Furthermore, the near constancy of the spectral index of nonthermal radio continuum emission over large distances along the minor axis in the halo of edge-on galaxies is most naturally explained by an advective transport velocity of relativistic electrons (along with the nucleons) that is ever increasing with distance from the Galactic plane (Breitschwerdt 1994).

In the disk of spiral galaxies, the regular magnetic field is following roughly the spiral arms and is therefore mostly parallel to the disk, with noticeable deviations in some regions where outflow is expected. Here, also a regular vertical component seems to be present (e.g. Hummel et al. 1988), which has been detected in a number of galaxies like NGC 4631, NGC 5775 (Tüllman et al. 2000), and NGC 4217. Multi-wavelength observations of the galaxy NGC 253 show a local correlation between non-thermal radio continuum,  $H\alpha$  and X-ray emission near the disk-halo interface in off-nuclear regions (Dettmar 1992; M. Ehle, private communication). This also spatially coincides with enhanced star formation activity in the disk as can be seen from FIR data.

Since the disk is not fully ionized in contrast to the halo and since waves are efficiently dissipated there by ion-neutral damping, the most important contribution to the random field in the disk is by turbulent mass motions, induced by supernova explosions and other stellar mass loss activity. Thus the wave spectrum will be very different from the one in the halo, where self-excited waves subject to nonlinear wave damping (Dogiel et al. 1994; Ptuskin et al. 1997), satisfying the gyro-resonance condition, dominate. Consequently, the averaged diffusion coefficient will be different in the Galactic disk and the halo (see Sect. 4).

Therefore, we believe that anisotropic diffusion, together with radially varying advection, is the most general and most probable mode of CR transport to occur.

We investigate the CR transport processes of diffusion and advection and discuss the possibility of flattening radial CR source gradients of a *given SNR distribution* (despite observational uncertainties) by particle propagation. In our view it is essential using the “natural” boundary condition when *calculating* the response of CR transport to a given CR source distribution (whatever its observational limitations may be at the present time). This is in contrast to *adjusting* the source distribution a posteriori. To implement the transport processes properly we shall allow for radially varying advection, anisotropic diffusion, (different values of the diffusion coefficient parallel and perpendicular to the disk) and the appropriate boundary conditions to employ a cosmic ray distribution and then to calculate from these the resulting spatial distribution of CRs.

In Sect. 4 we discuss the question of anisotropic CR diffusion and in Sect. 5 we introduce a simple model that describes the *observed* CR source distribution. In the following Sect. 6 we show heuristically (and in Sect. 8 also analytically) how a radially varying CR source distribution induces variations in the CR energy density, which in turn leads to a radial variation of the diffusion-advection boundary,  $z_C$ , and the outflow velocity, respectively, and thus to a tendency to *flatten* the radial CR distribution and hence the  $\gamma$ -ray emissivity gradient. In Sect. 7 we demonstrate by numerical calculations how such a source distribution will naturally generate a radially varying outflow velocity. In Sect. 8 we discuss in detail models of different complexity for advective-diffusive transport with radially varying outflow velocity, and show analytically how in each case for a *given* CR source distribution its radial signature on the energetic particle and  $\gamma$ -ray distribution is reduced. The most advanced of these models include a dependence of galactic wind velocity on the CR source strength. In addition a full analytic solution of the 3-dimensional diffusion-advection equation in axisymmetry for a given realistic velocity dependence  $u(r, z)$ , parallel and perpendicular to the Galactic disk similar to the one derived in Sect. 7, is calculated. In Sect. 9 the source contributions to the “diffuse”  $\gamma$ -ray background at TeV energies are taken into account and shown to be highly significant. This should allow an empirical test of our theoretical picture. In Sect. 10 we discuss and summarize our results. A number of detailed calculations can be found in the Appendices A, B and C.

#### 4. Anisotropic diffusion coefficient

In most models of diffusive CR propagation, the diffusion tensor is approximated by a scalar quantity  $D$ , representing spatially uniform transport,  $D = D_0 E^\alpha$ , where  $\alpha = 0.5\text{--}0.6$  describes the energy dependence. However, there are good reasons why the diffusion coefficient may be anisotropic.

The propagation of CRs in the interstellar medium is mainly determined by their interaction with electric and magnetic fields. CRs interact strongly with fluctuations of the magnetic field (MHD-waves) and are scattered by them in pitch angle. In the simplest case the total magnetic field consists of two components and can be written as

$$B = B_0 + \delta B, \quad (2)$$

where  $B_0$  is the average large scale magnetic field and  $\delta B$  is the field of small scale fluctuations.

Effective scattering of particles by these fluctuations occurs when the interaction is resonant, i.e. when the scale of the fluctuations in the magnetic field  $B_0$  is of the order of the particle gyroradius. This leads to a stochastic motion of particles through space; the associated diffusion coefficient  $D_{\parallel}$  along the magnetic field  $B_0$  is of the order of

$$D_{\parallel} \sim v L_{\parallel}, \quad (3)$$

where  $v$  is the particle velocity. The value  $L_{\parallel} \sim v/\nu$  is the transport length of the particle along the magnetic field lines, and  $\nu$  is the rate of resonant particle scattering. The main assumption of this description is that the fluctuation amplitude is much less than the average magnetic field

$$\delta B \ll B_0. \quad (4)$$

The displacement of a charged particle perpendicular to the regular magnetic field  $B_0$  due to scattering is therefore small:

$$D_{\perp} \sim D_{\parallel} \cdot \left( \frac{r_g}{L_{\parallel}} \right)^2, \quad (5)$$

i.e.,

$$D_{\parallel} \gg D_{\perp}, \quad (6)$$

where  $r_g$  is the particle gyroradius, and  $r_g \ll L_{\parallel}$ .

The situation is more complex if there exists also a large scale random magnetic field  $\Delta B$  whose scale is much larger than the particle gyroradius:

$$B = B_0 + \Delta B + \delta B. \quad (7)$$

In this case the diffusion transverse to the magnetic field  $B_0$  occurs due to the divergence of the particle trajectories, which is much faster than the resonant diffusion from Eq. (5).

The procedure to derive the transport equation for CRs in this case was described, e.g. by Toptygin (1985), who showed that the maximum value of  $D_{\perp}$  is:

$$D_{\perp} \sim D_{\parallel} \left( \frac{\Delta B}{B_0} \right)^2. \quad (8)$$

Thus, diffusion in the Galaxy is quasi-isotropic only in the case  $\Delta B \sim B_0$ .

A more precise analysis (see Berezhinsky et al. 1990, Chap. 9) shows, however, that in the interstellar medium the correlation between the components of the diffusion

tensor leads to an effective perpendicular diffusion coefficient:

$$D_{\perp}^{\text{eff}} \sim 0.1 \cdot D_{\parallel}. \quad (9)$$

Observations show that in the Galactic disk the large scale magnetic field is typically parallel to the disk, whereas in the halo also a significant perpendicular component may exist, as it has been observed in the case of the edge-on Sc galaxy NGC 4631. Therefore one can expect  $D_z \ll \kappa_r$  in the disk, and  $D_z \gg \kappa_r$  in the halo<sup>1</sup>, with  $D_z$  and  $\kappa_r$  being the components of the diffusion tensor perpendicular and parallel to the Galactic plane. Thus, in general, CRs spend a considerable amount of their transport time in the halo, subject to *anisotropic* diffusion.

### 5. A simple model for the galactic CR source distribution

The inference on the spatial distribution of CR sources from *direct* observations is plagued by a number of problems. From energy requirements for the bulk of CRs below  $10^{15}$  eV, it is known that the only non-hypothetical Galactic candidates for the sources are SNRs and pulsars, with global energetic requirements favouring the former. SNRs can be best studied in the radio continuum and in soft X-rays, but as low surface brightness objects larger and older remnants are systematically missed. Since samples are usually flux limited, the more distant objects will be lost as well. Pulsars on the other hand should be present in the Galaxy in large numbers. However they are only detectable if their narrow beams happen to cross the line of sight of the observer or, in X-rays, as isolated old neutron stars; so far only four candidates are known from the ROSAT All-Sky Survey (Neuhäuser & Trümper 1999). Therefore selection effects will bias samples heavily in both cases.

Based on the observations of SNRs by Kodeira (1974) and pulsars by Seiradakis (1976), Stecker & Jones (1977) have given a simple radial Galactic distribution of the form

$$Q_1(x) = q_0 x^a \exp(-bx), \quad (10)$$

where,  $Q_1(x)$  is a SNR surface density in  $x$ , with  $x = r/R_{\odot}$ , and  $a$  and  $b$  are matched to the observations. Here we adopt  $a = 1.2$  and  $b = 3.22$ . Since both SNRs and pulsars are associated with Population I objects, it is reassuring that  $a$  and  $b$  are very similar for both classes of objects.

To determine the proportionality constant  $q_0$  for the distribution given in Eq. (10), we use the results obtained by Leahy & Xinji (1989) who used the catalogue of Li (1985) derived from radio observations. Leahy & Xinji (1989) considered shell-type SNRs and applied empirical correction factors due to the incompleteness of the flux limited sample. The spatial distribution thus obtained shows a peak at 4–6 kpc from the Galactic center (see Fig. 1), assuming an overall rotational symmetry. A more

<sup>1</sup> Note that in the disk,  $\kappa_r$ , and in the halo,  $D_z$ , are both *parallel* to the large scale regular magnetic field direction.

systematic study has recently been undertaken by Case & Bhattacharya (1998), who have made a careful analysis of an enhanced Galactic SNR sample, using an improved  $\Sigma - D$  relation. These authors find a peak in the distribution at around 5 kpc<sup>2</sup> and a scale length of  $\sim 7$  kpc, thus confirming the gross features of the older work. The number of SNRs in an annulus of width  $dx$  is given by

$$\begin{aligned} dN &= Q_1(x) 2\pi x dx \\ &= 2\pi q_0 x^{a+1} \exp(-bx) dx, \end{aligned} \quad (11)$$

and thus the total number of SNRs in the disk of radius  $\sim 18$  kpc is

$$\begin{aligned} N &= 2\pi \int_0^{x_g} q_0 x^{a+1} \exp(-bx) dx \\ &\approx 2\pi q_0 \int_0^{x_g} x^2 \exp(-bx) dx \\ &= 2\pi q_0 \left[ -\exp(-bx) \left( \frac{x^2}{b} + \frac{2x}{b^2} + \frac{2}{b^3} \right) \right]_0^{x_g} \\ &\approx 0.35 q_0, \end{aligned} \quad (12)$$

for  $x_g = 1.8$ ,  $a \approx 1$  and  $b = 3.22$ . Numerical integration of Eq. (12) yields  $N \approx 0.33 q_0$ .

On the other hand, the total number of SNRs that should be observable at present is their production rate  $\theta$  times their average life time  $\tau_{\text{SN}}$  before they merge with the hot intercloud medium and lose their individual appearance, or observationally escape the detection limit. The rate at which SNe occur in the disk is  $2.2 \pm 1.3$  per century for randomly exploding stars (van den Bergh 1990, 1991) and 0.45 per century for explosions occurring in OB associations (Evans et al. 1989), giving a total SN rate in the Milky Way disk of  $\theta = 2.65$  per century. The total number of SNRs in the disk is then given by

$$N = \theta \tau_{\text{SN}}. \quad (14)$$

For  $\tau_{\text{SN}} = 1.83 \times 10^4$  years we reproduce the value given by Leahy & Xinji (1989), who estimate  $N = 485 \pm 60$  for Galactic SNRs with a limiting surface brightness of  $\Sigma \geq 3 \times 10^{-22} \text{ W m}^{-2} \text{ Hz}^{-1} \text{ sr}^{-1}$ . From Eq. (13) we obtain:  $q_0 = 1386 \pm 171$ .

Dragevich et al. (1999) have analyzed also the radial distribution of SNe in a sample of 218 *external galaxies* of different Hubble types, corrected for inclination angle. The data were sorted into radial bins and the numbers converted into SNe surface densities. They showed that the radial SN surface distribution can be well fitted by an exponential radial decrease of the form

$$S(R) = \sigma_c e^{-R/R_{\text{sc}}}, \quad (15)$$

with  $\sigma_c = 350$ . Taking a sub-sample of 36 Sb-Sbc galaxies, they were able to derive a value of  $R_{\text{sc}} = 5.4$  kpc for the exponential scale length of the Milky Way as a representative Sb-Sbc galaxy. The number of SNe derived is

<sup>2</sup> The difference is due to the fact that with the older value of  $R_{\odot} = 10$  kpc in Eq. (10) the peak of the distribution appears at  $r_{\text{max}} = \frac{a}{b} R_{\odot} \sim 4$  kpc.

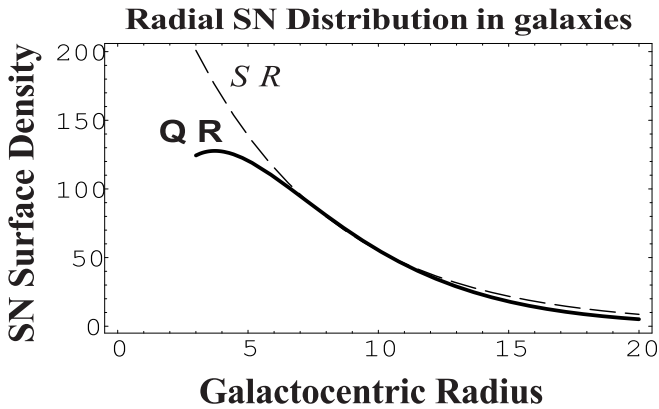


**Fig. 1.** Surface density of SNRs and supernovae, respectively, in galaxies as a function of Galactocentric distance  $R$ . The solid curve,  $Q(R)$ , gives a fit to the SNR distribution of the Milky Way and is given by  $Q(R) = 87.45R^{1.2} \exp[-0.322R]$ , whereas the dashed curve is a fit to the extragalactic supernova distribution by Dragicevich et al. (1999), given by  $S(R) = 350 \exp[-0.185R]$ . Note the excellent agreement in the exponential decrease of  $Q(r)$  and  $S(R)$  for  $5 < R < 20$  kpc.

consistent with historical records of Galactic SNe within 4 kpc from the Sun. In Fig. 1 it is shown that both the exponential decrease and, interestingly, but rather fortuitously, also the absolute numbers in the SN surface density agree fairly well for  $R > 5$  kpc with the earlier derived relation (10) for the SNR surface density.

Therefore the value calculated for the proportionality constant,  $q_0$ , provides a reliable estimate for the number of Galactic SNRs in a circular ring at a distance  $R$ .

It should be emphasized that the SNR lifetime,  $\tau_{\text{SN}}$ , does not enter the analysis of Sect. 7, (see Eq. (21)), since it is only the CR production rate and hence the SNR rate per unit volume that determines the truly diffuse  $\gamma$ -ray emissivity.

## 6. Flattening of the radial $\gamma$ -ray emissivity gradient

In the following we will argue that the CR propagation picture needs to be changed for two physical reasons. Firstly, as we have already pointed out, diffusive transport in the disk and in the halo is not the same due to a different magnetic field geometry and to different wave excitation and damping mechanisms. Thus *anisotropic* diffusion seems to be rather the rule than the exception. Secondly, advection of CRs is the dominant transport mode above a certain transition boundary located at  $(R_C, z_C)$ , with  $z_C = z_C(r)$  varying with Galactic radius.

More specifically, we consider SNRs as the primary sources for the Galactic CRs. Each remnant results from an energy deposition of  $E_{\text{SN}} \simeq 10^{51}$  erg, which is converted into relativistic particles with a certain efficiency  $\nu \sim 0.1$ – $0.5$  (Drury et al. 1989; Berezhko & Völk 2000); the individual value of  $\nu$  is poorly known from theory due to uncertainties in the injection process and depends e.g., on the value and orientation of the circumstellar magnetic field. SNe exploding inside a superbubble, i.e. a hot tenu-

ous medium, initially generate low Mach number shocks, which are less efficient in accelerating particles. After a time of the order of the sound crossing time, however, the shock impinges on the much colder and denser surrounding shell and becomes progressively stronger thereby accelerating particles more efficiently; this should to lowest order compensate for the initially decreased efficiency in the hot ambient medium. We would expect that due to the continuous energy input by successive SN explosions also a long lived shock would be able to accelerate particles to energies in excess of  $10^{14}$  eV, albeit adiabatic energy losses would become more and more severe with time. Since the diffusion coefficient of CRs increases with energy, advective transport of particles significantly above 1 GeV will be the dominant mode of transport only at larger distances from the Galactic plane. Therefore these particles will quickly fill an extended halo and not generate many  $\gamma$ -rays in the disk via  $\pi_0$ -decay.

Bykov & Fleishman (1992) have argued that successive explosions inside a bubble can generate strong turbulence, which should transform a significant amount of the total free energy to cosmic rays. However, at the same time the injection rate at the shocks may be reduced as a result of shock modification due to previously generated CR particles. With the details of the acceleration mechanism in superbubbles being still debatable, we believe that to lowest order there is no difference in the overall energy transfer from thermal plasma to CRs, if a SN explodes inside a superbubble or just forms a single remnant. Thus the energy production rate of CRs should be roughly proportional to the number of SN explosions, regardless whether they occur in the general ISM or inside a superbubble. The numerical difference in the derived CR energy density (and CR pressure) (cf. Eqs. (18) and (17)), however, between treating particle acceleration in superbubbles as equal to single remnants, and disregarding acceleration in superbubbles altogether, is small. According to the previous section it amounts to a factor  $\theta_{\text{tot}}/\theta_{\text{SNR}} = 2.65/2.2 \approx 1.2$ , and is therefore well below the uncertainty in the acceleration efficiency  $\nu$ . In the following, we tend to be conservative and retain a low value of  $\nu = 0.1$ .

Using the results from Sect. 5 we can estimate the local number of SNRs within a circular ring of the Galaxy with a width of, say, 2 kpc. Relating the SN rate directly to the number of observable SNRs by Eq. (14) and writing (cf. Eq. (11))

$$Q_1(x) = \frac{\Delta N(x)}{2\pi x \Delta x}, \quad (16)$$

we can now define the SNR rate per unit radial confinement volume,  $\eta(x)$ , by

$$\begin{aligned} \eta(x) &= \frac{\Delta N(x)}{\tau_{\text{SN}} \Delta V} \\ &= \frac{\theta Q_1(x)}{N z_C R_\odot^2}. \end{aligned} \quad (17)$$

The local CR energy density,  $\epsilon_C$  in the disk at  $z \approx 0$ , can then be estimated to be

$$\epsilon_C(x) = \frac{\gamma_C}{\gamma_C - 1} P_C(x) = \frac{1}{2} \eta(x) E_{\text{SN}} \nu \tau_{\text{esc}}, \quad (18)$$

with  $\Delta V(x) = 2\pi x \Delta x z_C R_\odot^2$ , and  $\tau_{\text{esc}}$  being the local diffusive CR storage volume and time, respectively; the factor  $\frac{1}{2}$  accounts for one half-space, e.g.  $z > 0$ . The CR pressure in the disk is denoted by  $P_C(x)$  and  $\gamma_C \approx 4/3$  is the specific heat ratio for the CRs. Working in the framework of an average transition boundary,  $z_C$ , which divides space below and above in purely diffusion and advection regions, respectively, the probability for particles at  $z > z_C$  to return and hence contribute to the CR pressure in the disk becomes exponentially small. We have therefore used  $z = z_C$  as the vertical extension for the CR storage volume. As we can see from Eq. (17),  $\eta(x)$ , depends on the local and total number of sources and the global SN rate, but not on the SNR life time. The vertical extent of the diffusion-advection boundary  $z_C$  is determined by the balance of diffusive and advective CR flux at this vertical distance, i.e. to lowest order by

$$z_C \sim \frac{D}{V} = \frac{D}{u_0 + V_{A0}}, \quad (19)$$

and the local CR escape time is

$$\tau_{\text{esc}}(x) \sim \frac{z_C^2(x)}{D} \sim \frac{D}{(u_0(x) + V_{A0}(x))^2}. \quad (20)$$

Thus the radial CR pressure variation is given by

$$\begin{aligned} P_C(x) &= \frac{\gamma_C - 1}{2\gamma_C} \frac{\eta(x) \nu E_{\text{SN}} z_C}{(u_0(x) + V_{A0}(x))}, \\ &= \frac{\gamma_C - 1}{2\gamma_C} \frac{\theta Q_1(x) \nu E_{\text{SN}}}{N R_\odot^2 (u_0(x) + V_{A0}(x))}. \end{aligned} \quad (21)$$

It is easy to show that Eq. (21) follows directly from the kinetic equation for CRs, as can be seen from Eq. (47).

The diffuse  $\gamma$ -ray intensity resulting from  $\pi^0$ -decay photons is

$$I_\gamma \propto \int_0^l n_C n_H dl \sim \langle n_C \rangle \langle n_H \rangle l, \quad (22)$$

with  $\langle n_C \rangle$  and  $\langle n_H \rangle$  being the line-of-sight averaged CR and hydrogen number density, respectively, and  $l = \sqrt{z_C^2 + (r - R_\odot)^2}$  is the line of sight. From Eq. (21) we have

$$n_C \propto P_C(x) \propto \frac{Q_1(x)}{u_0 + V_{A0}}, \quad (23)$$

disregarding the changes in the CR distribution function due to energy-dependent diffusion.  $n_H$  is an observationally fixed quantity, for which we have to use its line of sight averaged value (see Eq. (22)) if we are interested in quantitative calculations of the  $\gamma$ -ray intensity; here we are primarily concerned with the radial variations of  $I_\gamma$ .

In order to obtain  $n_C \approx \text{const}$  for a weak  $\gamma$ -ray gradient, we should assume that

$$(u_0 + V_{A0}) \propto Q_1(x), \quad (24)$$

if  $V \sim \text{const}$ ; if  $V = V_0 z$ , we have  $z_C \sim \sqrt{D/V_0}$  and therefore should require

$$(u_0 + V_{A0}) \propto Q_1^2(x). \quad (25)$$

Combination of Eqs. (20) and (24) leads to

$$\tau_{\text{esc}} \propto \frac{D}{Q_1^2(x)}. \quad (26)$$

All other things being equal, a locally enhanced CR production rate should therefore lead to a reduced CR escape time with only a small effect on the diffuse  $\gamma$ -ray intensity.

## 7. Radially dependent cosmic ray driven outflows

As we have deduced in the last section, the CR pressure  $P_C(x)$  in the disk is a radially dependent quantity, and therefore we expect the outflow velocity,  $u(x)$ , and the mass loss rate,  $\dot{m}(x)$ , to be also radially dependent. In an earlier paper (Breitschwerdt et al. 1991) we have shown that such a behaviour already exists as a consequence of the radial dependence of the gravitational potential. The net result was a monotonic decrease (increase) of terminal velocity (mass loss rate) with increasing Galactic radius for a radially constant mass density,  $\rho_0$ . Now we have superposed the radial variation of the CR source density  $Q_1(x)$  and investigate in the following how this changes the outflow.

However, Eq. (21) is an *implicit* equation, since  $P_C(x)$  depends on  $u_0(x) + V_{A0}(x)$ , which in turn depends on the energy density available in CRs, i.e.  $\epsilon_C(x)$  and thus  $P_C(x)$  itself, to drive the outflow. To that end we have performed *self-consistent* galactic wind calculations of the fully nonlinear equations, in which for a given gravitational potential of the Milky Way, and a relativistic CR gas ( $\gamma_C = 4/3$ ), together with a spatially averaged mass density  $\varrho(x) \sim \varrho_0 = 1.67 \times 10^{-27} \text{ g cm}^{-3}$ , an average thermal pressure  $P_g(x) \sim P_{g0} = 2.76 \times 10^{-13} \text{ dyne cm}^{-2}$ , an averaged halo magnetic field  $B(x) \sim B_0 = 1 \mu\text{G}$ , and a small average level of wave amplitude  $\delta B(x)/B(x) \sim \delta B_0/B_0 = 0.1$ , the advection-diffusion boundary  $z_C(x)$ ,  $P_C(x)$  and  $u_0(x) + V_{A0}(x)$  are calculated self-consistently, using  $g_0 = 1492$ , the value derived from the numerical integration of Eq. (12) (see Sect. 5). The form of the potential (including, disk, bulge and dark matter halo) and the opening of the flux tube due to geometrical divergence are the same as used by Breitschwerdt et al. (1991). We have used a radial grid for our calculations in the Galactic radius interval from 0.5–12 kpc, with spacings of 0.5 kpc. The net radial dependence of the outflow velocity we obtained from our numerical calculations is shown in Fig. 2, and its  $r$ - and  $z$ -dependence in Fig. 7. The outflow velocity  $u_0 + V_{A0}$  in Fig. 2 (solid line) for a fixed Galactic frame of reference at the radially varying transition boundary  $z_C(r)$ , shows a similar convex shape as the source distribution  $Q_1(x)$  (short dashed curve), although much less pronounced. This is due to the fact, that the decrease of the gravitational potential, as can be seen from the escape speed,  $v_{\text{esc}} = \sqrt{-2\Phi_0}$ , with  $\Phi_0 = \Phi_b + \Phi_d + \Phi_h$  for

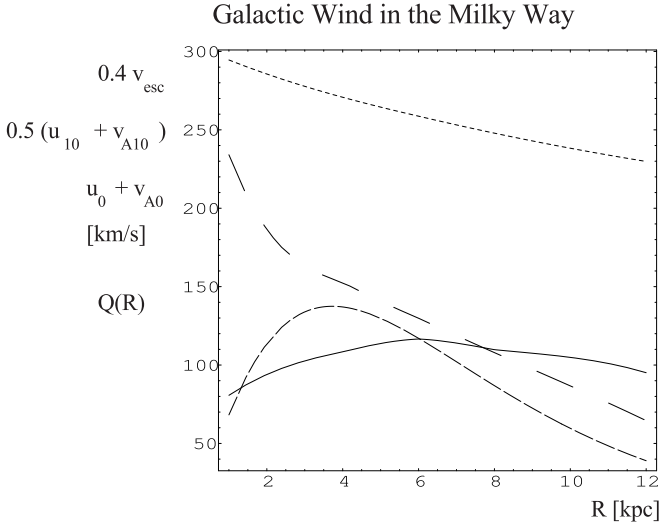


**Fig. 2.** Escape speed,  $v_{\text{esc}} = \sqrt{-2\Phi_0}$ , of the Galaxy (dotted curve), outflow velocity,  $u_{10} + v_{A10}$ , at a vertical distance of  $z = 10$  kpc (long dashed curve), and outflow velocity,  $u_0 + v_{A0}$ , at reference level,  $z_C$  (solid curve), respectively, as seen in a fixed frame of reference, and the supernova distribution function (short dashed curve),  $Q(R)$ , (see Eqs. (10) and (13)), as a function of Galactocentric radius  $R$ . Curves have been scaled down by the factors indicated on the vertical axis to fit into one diagram. For boundary conditions of self-consistent galactic wind calculations see text.

bulge, disk and halo contributions, respectively, (dotted curve in Fig. 2), keeps the outflow velocity from dropping off too rapidly with increasing Galactocentric distance. Therefore, even a uniform SNR distribution would enforce a radially varying outflow velocity, as has been shown in Fig. 7 of Breitschwerdt et al. (1991). The radial variation of the outflow velocity at a distance of  $z = 10$  kpc from the disk,  $u_{10} + V_{A10}$ , is shown by the long dashed curve, which both shows the transition from the flow velocity at reference level  $z_C$  to the escape speed, and also a roughly  $1/r^2$ -dependence, which we will use in our analytical treatment later (cf. Eq. (99)).

It can be seen from comparison of  $z_C(r)$  and  $u_0(r) + V_{A0}(r)$ , as obtained from the fully nonlinear calculations, that the simple ansatz of Eq. (19) is indeed fulfilled. The functional dependence of  $z_C(r)$  with radius is straightforward to understand. Close to the Galactic centre, the gravitational pull is strongest, as can be seen from  $v_{\text{esc}}$  in Fig. 2; since we chose all other quantities being the same across the disk (constant density, thermal pressure, magnetic field strength), the outflow velocity, and hence mass loss rate, are smallest here. Equation (19) then tells us, that  $z_C(r)$  must be largest. At the outer parts of the Galaxy, the gravitational field becomes weaker, but also the source distribution, and hence the CR pressure, decrease exponentially, and so the outflow velocity (cf. Fig. 2) also decreases, and  $z_C(r)$  must increase again (see Fig. 3). It is noteworthy that the maximum of  $u_0(r) + V_{A0}(r)$  and the minimum of  $z_C(r)$  at  $r \sim 6$  kpc do not coincide with the maximum of  $Q_1(r)$  and  $P_C(r)$ ,

Variation of Reference Level with Galactic Radius

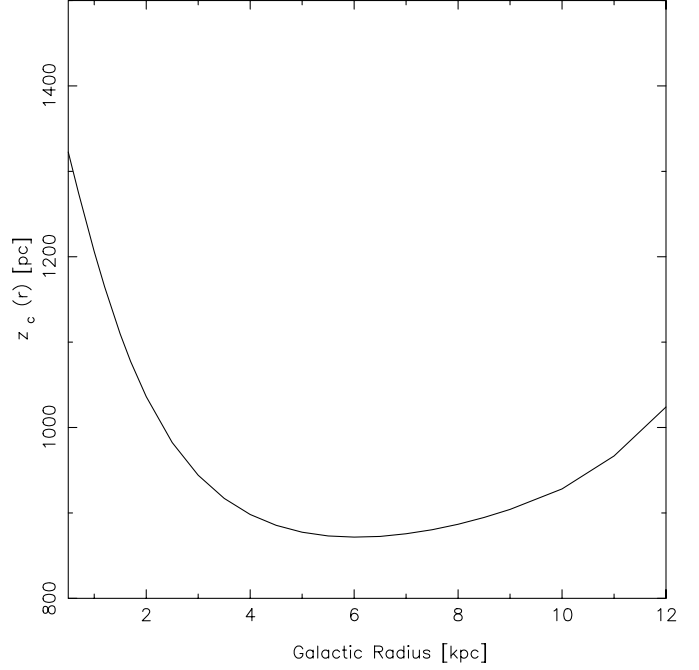


**Fig. 3.** Dependence of the diffusion-advection boundary,  $z_C(r)$ , on Galactocentric radius  $r$ . The location of  $z_C$  at any radius is defined by the balance of diffusive and advective CR fluxes. The curve shown here has been obtained from self-consistent galactic wind calculations (see text).

respectively, at  $r \sim 3-4$  kpc. This must be a consequence of the interplay between the gravitational field and the source distribution in the fully nonlinear equations (cf. Breitschwerdt et al. 1991).

Finally we mention that the choice of constant boundary conditions across the Galactic disk is a conservative one. In reality we should also enhance the thermal temperature and pressure in regions of higher supernova activity. The net effect would be a more pronounced peak in outflow velocity and a deeper minimum in  $z_C(r)$ , respectively, and therefore an even “better” quantitative proportionality between  $u_0(r) + V_{A0}(r)$  and  $Q_1(r)$  according to Eq. (24).

## 8. Models of advective and anisotropic diffusive CR transport

In the following we discuss several advection models (some including also anisotropic spatial diffusion), in which we examine in detail the ideas presented in Sect. 6. We show that for a given radial CR source distribution function  $f_1(r) \propto Q_1(r)$ , we can find a function  $f_2(r) \propto V(r)$ , for which the effect of the radially varying Galactic wind velocity leads to an almost uniform CR distribution in the disk. We refer to relations  $f_2(r) = F(f_1(r))$  as “compensation equations”. It is thus possible to explain the observational data by pure CR propagation effects.

To fix ideas, we start out with a functional relation for the Galactic CR source distribution of the form

$$Q(z, r, E) = K(E) f_1(r) \delta(z), \quad (27)$$

neglecting the thickness of the Galactic disk; here  $\delta(z)$  denotes the Dirac delta function. Then for a given source distribution function,  $f_1(r)$ , we try to find a wind structure of the form

$$V(r, z) = V(z) f_2(r), \quad (28)$$

which makes the CR distribution almost uniform. In the following we describe models of increasing complexity with respect to geometry and outflow velocity.

### 8.1. One-dimensional model with a constant galactic wind velocity

We start from the simplest one-dimensional CR transport model, which is an extreme case of anisotropic diffusion, since only propagation in the  $z$ -direction is allowed. In this case the galactocentric radius  $r$  is simply a parameter in the model.

The one-dimensional diffusion-advection equation for CR nucleons can be written as

$$\frac{\partial}{\partial z} \left( V(r, z) n - D \frac{\partial n}{\partial z} \right) - \frac{1}{3} \frac{dV}{dz} \frac{\partial}{\partial E} (E n) = Q(E, r, z), \quad (29)$$

where for simplicity we take the advection velocity to be constant and directed away from the Galactic plane

$$V(r, z) = \pm V_0 f_2(r) \Theta(\pm(z - z_C)). \quad (30)$$

Here  $\Theta(z - z_C)$  is the Heavyside step function, and the sign “+” corresponds to the velocity above, and the sign “-” to the one below the Galactic plane.

The boundary conditions for CRs are determined either by free escape into intergalactic space, if the density of electromagnetic fluctuations generated by the CR flux decreases fast enough (see Dogiel et al. 1994), or by CR advection in a galactic wind to infinity (Breitschwerdt et al. 1991; Ptuskin et al. 1997), if the level of fluctuations is high enough. Which of these cases is relevant for the Galaxy, is the subject of a separate investigation. Fortunately, CR spectra and densities in the disk are independent of the boundary conditions *far away* from the Galactic plane, if there is an outer region of advective transport. In the case we discuss here, it is assumed that the CR propagation region can be formally divided into a diffusion halo wrapping around the Galactic plane and an adjacent advection region, reaching out to intergalactic space. These two regions are separated by a boundary surface,  $z_C$ , at which both the CR density and the flux have to be continuous.

The sources are concentrated in the disk and are supposed to emit a power-law spectrum of particles

$$Q(E, r, z) = z_d K f_1(r) E^{-\gamma_0} \delta(z), \quad (31)$$

where  $z_d$  is the thickness of the Galactic disk and the coefficient  $K$  determines the CR production by SNRs in the disk.

The location of the transition boundary for a constant diffusion coefficient  $D$  and advection velocity  $V_0$  is determined in this approximation by

$$z_C = \frac{D}{V_0}. \quad (32)$$

Then for  $z < z_C$  the transport equation reads

$$-D \frac{d^2 n_d}{dz^2} = z_d K f_1(r) E^{-\gamma_0} \delta(z), \quad (33)$$

and for  $z \geq z_C$

$$\frac{d}{dz} (n_C V_0 f_2(r)) + \frac{1}{3} V_0 f_2(r) \delta(z - z_C) (\gamma_0 - 1) n_C = 0. \quad (34)$$

Since adiabatic energy losses do not change the particle spectral index,  $n \propto E^{-\gamma_0}$ . The solution of Eq. (33) is

$$n_d = C_1 + C_2 z \quad (35)$$

and the CR density is constant in the advection region,

$$n_C = C_0. \quad (36)$$

The constants can be determined from the boundary conditions at  $z = 0$

$$-D \frac{dn_d}{dz} = z_d K f_1(r) E^{-\gamma_0}, \quad (37)$$

and at  $z = z_C$  by continuity of the diffusive and advective CR fluxes

$$D \frac{dn_d}{dz} = V_0 f_2 n_C + \frac{V_0 f_2}{3} (\gamma_0 - 1) n_C. \quad (38)$$

Since at  $z = z_C$  also  $n_d = n_C$ , we obtain

$$n_C = \frac{3z_d K E^{-\gamma_0} f_1(r)}{V_0 (\gamma_0 + 2) f_2(r)}, \quad (39)$$

and therefore

$$n_d = z_d K f_1(r) E^{-\gamma_0} \left( \frac{3}{V_0 f_2(r) (\gamma_0 + 2)} - \frac{z - z_C}{D} \right). \quad (40)$$

We see that at  $z = 0$

$$n_d = \frac{z_d K f_1(r) E^{-\gamma_0} (\gamma_0 + 5)}{f_2 V_0 (\gamma_0 + 2)}, \quad (41)$$

and the “compensation” equation must have the form

$$f_1(r) = f_2(r), \quad (42)$$

for the CR particle density to be uniform, in other words, the radial dependence of the outflow velocity must be the same as that of the source distribution.

From Eq. (40) we can also estimate the total pressure,  $P_C$ , of CRs in the disk, which is

$$P_C = \int_{E_0}^{\infty} n_d(z=0, E) E \cdot dE \quad (43)$$

$$= \frac{z_d K f_1 E_0^{-(\gamma_0-2)} (\gamma_0 + 5)}{(\gamma_0 - 2) f_2 V_0 (\gamma_0 + 2)}. \quad (44)$$

The physical units of  $K$  are  $[K] = \text{erg}^{\gamma_0-1}/\text{s}$ , and  $KE_0^{-(\gamma_0-2)}$  equals the CR power in the Galactic disk, hence (neglecting constants of order unity)

$$KE_0^{-(\gamma_0-2)} \simeq \nu E_{\text{SN}} \frac{\theta}{N}. \quad (45)$$

On the other hand the normalized source distribution (cf. Eq. (16)) is equivalent to

$$\frac{Q_1(x)}{R_{\odot}^2} = \frac{\Delta N}{\Delta A_{\text{d}}} = \frac{f_1 \Delta V_{\text{d}}}{\Delta A_{\text{d}}} = f_1 z_{\text{d}}, \quad (46)$$

where  $A_{\text{d}}$  and  $V_{\text{d}}$  are the area and volume of the Galactic disk, respectively, and identifying  $V_0$  with  $u_0 + V_{\text{A}0}$ , Eq. (44) becomes

$$P_{\text{C}} = z_{\text{d}} f_1 \frac{KE_0^{-(\gamma_0-2)} (\gamma_0 + 5)}{(\gamma_0 - 2) f_2 V_0 (\gamma_0 + 2)} \simeq \frac{Q_1(x)}{R_{\odot}^2} \cdot \nu E_{\text{SN}} \frac{\theta}{N(u_0 + V_{\text{A}0})}, \quad (47)$$

which corresponds to Eq. (21), thus verifying the validity of the intuitively derived relation between CR pressure, source distribution and Galactic SN rate in a Galactic wind flow.

### 8.2. One-dimensional model with $z$ -dependence of the wind

Based on the conclusions of the previous sections, we can generalize the one-dimensional solution obtained by Bloemen et al. (1993), taking into account radial variations of the sources and the wind velocity. Let us suppose that the advection velocity has the form

$$V(z, r) = 3\tilde{V}_0 z f_2(r); \quad (48)$$

the solution of Eq. (29) is then given by

$$n(z=0, r) \simeq A \frac{K f_1(r)}{\sqrt{D \tilde{V}_0 f_2(r)}} E^{-\gamma}, \quad (49)$$

where  $A$  is a constant; note that  $\tilde{V}_0$  is a typical time constant (e-folding time) of the flow.

We find that a vanishing radial dependence of the CR distribution,  $n = \text{const}$ , can be obtained if

$$f_1^2(r) = f_2(r). \quad (50)$$

In these simple models the size of the halo can be derived only locally, because global or large-scale characteristics, like e.g. the CR distribution along the Galactic plane, are independent of the CR propagation itself.

These simple analytical solutions of the one-dimensional transport equation show that the main effect, which formally leads to the ‘‘compensation’’, is a curved transition boundary between diffusion and advection regions, i.e.

$$z_{\text{C}}(r) \sim \frac{D}{V(r)}; \quad (51)$$

note that such a behaviour is indeed apparent from Figs. 2 and 3. The main point here is that the compensation effect is a consequence of the  $r$ -dependence of the CR life-time,  $z_{\text{C}}^2/D \sim D/V^2(r)$ .

In the framework of the pure one-dimensional model it is unimportant how far from the Galactic plane the boundary  $z_{\text{C}}(r)$  is, but as we shall see, this figure will be essential for the three-dimensional case.

### 8.3. Three-dimensional axisymmetric model with radial velocity dependence

To demonstrate the effect of radial changes of the boundary  $z_{\text{C}}(r)$  between regions of diffusive and advective propagation of CRs, we investigate the diffusion-advection equation with a given radial dependence of the wind velocity and the source density in a more realistic cylindrical geometry (axial symmetry, i.e.  $\partial/\partial\varphi \equiv 0$ ) with the velocity varying as

$$V(r) = \frac{V_0}{r} = V_0 f_2(r), \quad (52)$$

and the source distribution as

$$Q(r, z) = \frac{Q_0}{r^\alpha} = Q_0 f_1(r). \quad (53)$$

Then the equation for the CR distribution function we have to solve reads

$$\frac{V_0}{r} \frac{\partial n}{\partial z} = D_z \frac{\partial^2 n}{\partial z^2} + \kappa_r \frac{1}{r} \frac{\partial}{\partial r} \left( r \frac{\partial n}{\partial r} \right) + \frac{Q_0}{r^\alpha} \delta(z), \quad (54)$$

where we have stressed the anisotropic diffusion by two different constant diffusion coefficients in the radial and perpendicular direction,  $\kappa_r$  and  $D_z$ , respectively. Note that  $V_0$  has the same dimensions as the diffusion coefficients, and that  $n(r, z)$  is the particle distribution function in phase space. The boundary conditions at  $z = 0$  are implicitly included in Eq. (54). Here we treat a special case of radial variation of the boundary  $z_{\text{C}}$ :

$$z_{\text{C}}(r) \sim r \frac{D_z}{V_0}, \quad (55)$$

corresponding to the velocity dependence given in Eq. (52). Comparison with Figs. 2 and 3 shows that such a behaviour may indeed represent the outer Galaxy, where the outflow velocity decreases with increasing radius and the distance of the boundary  $z_{\text{C}}$  from the Galactic disk increases accordingly.

Equation (54) can be solved analytically if we restrict ourselves to self-similar solutions, in which the distribution function does not vary with  $r$  and  $z$  independently. The price we have to pay is that there is no unique solution that covers both  $0 \leq r < \infty$  and  $0 \leq z < \infty$ . Instead a similarity solution is found for  $z \rightarrow 0$  and  $r > 0$ , and one for  $z > 0$ , which have to match in overlapping regions. We start out with the latter one, applying a transformation of independent variables of the form

$$\xi = \sqrt{\frac{D_z}{\kappa_r}} \frac{r}{z}, \quad (56)$$

and introducing the function

$$\phi(\xi) = z^{-\mu} n(z, r). \quad (57)$$

Equation (54) in terms of  $\phi$  and  $\xi$  then reads:

$$\begin{aligned} \xi(1 + \xi^2) \frac{\partial^2 \phi}{\partial \xi^2} + (b_1 + b_2 \xi + b_3 \xi^2) \frac{\partial \phi}{\partial \xi} \\ + (b_4 + b_5 \xi) \phi - \frac{Q_0}{\kappa_r} \frac{r^{2-\alpha}}{z^{1+\mu}} \delta(\xi - \infty) = 0, \end{aligned} \quad (58)$$

where the coefficients are given by

$$\begin{aligned} b_1 = 1, \quad b_2 = \frac{V_0}{\sqrt{\kappa_r D_z}}, \quad b_3 = -2(\mu - 1) \\ b_4 = -\frac{V_0 \mu}{\sqrt{\kappa_r D_z}}, \quad b_5 = \mu(\mu - 1). \end{aligned} \quad (59)$$

This equation can be cast into a self-similar form for two sets of the parameters  $\alpha$  and  $\mu$ :  $\alpha = 2$ ,  $\mu = -1$ , and  $\alpha = 1$ ,  $\mu = 0$ .

We can derive an analytical solution of this equation in the form (see Bakhareva & Smirnova 1980)

$$\phi(\xi) = K(1 + \xi^2)^C \exp(A \arctan \xi), \quad (60)$$

where  $K$  is a constant determined by the CR source power.

The unknown coefficients  $\mu$ ,  $C$  and  $A$  are determined from the system of algebraic equations which one can obtain from Eq. (58) by equating the coefficients for the different powers of  $\xi$  to zero. The resulting system of algebraic equations is given by

$$Ab_1 + b_4 = 0 \quad (61)$$

$$2C(1 + b_1) + A(A + b_2) + b_5 = 0 \quad (62)$$

$$2C(2A + b_2) - A(2 - b_3) + b_4 = 0 \quad (63)$$

$$2C(2C - 1 + b_3) + b_5 = 0. \quad (64)$$

We note that this system for the unknowns  $A$ ,  $C$  and  $\mu$  is overdetermined; therefore we have to check for consistency.

From the system of Eqs. (61)–(64) it can be deduced that

$$A = \frac{V_0 \mu}{\sqrt{\kappa_r D_z}}, \quad (65)$$

$$C = \frac{\mu}{2}, \quad (66)$$

$$\mu_1 = 0, \quad (67)$$

$$\mu_2 = -1. \quad (68)$$

It can be verified that these solutions are all consistent. However,  $\mu = 0$  implies  $A = 0$  and  $C = 0$ , and hence does not yield any physical solution. Taking  $\mu = -1$  gives  $C = -\frac{1}{2}$ . Therefore the solution is given by

$$\phi = K(1 + \xi^2)^{-1/2} \exp(A \arctan \xi), \quad (69)$$

where the constant  $K$  is determined from the conservation of particle flux at  $\xi = 0$ .

The limit  $z \rightarrow \infty$  corresponds to  $\xi \rightarrow 0$  so that

$$\begin{aligned} \lim_{\xi \rightarrow 0} \phi(\xi) &= \lim_{\xi \rightarrow 0} K(1 + \xi^2)^{-1/2} \exp(A \arctan \xi) \\ &= K = \frac{Q_0}{V_0}, \end{aligned} \quad (70)$$

because at large distances from the disk ( $z \rightarrow \infty$ ), the particle transport is completely determined by advective transport, and the number of particles ejected by the sources is conserved.

The full solution of Eq. (54) reads

$$\begin{aligned} n(r, z) &= \frac{Q_0}{V_0 \left( z^2 + \frac{D_z}{\kappa_r} r^2 \right)^{1/2}} \\ &\times \exp \left\{ -\frac{V_0}{\sqrt{\kappa_r D_z}} \left( \arctan \left[ \sqrt{\frac{D_z}{\kappa_r}} \frac{r}{z} \right] \right) \right\}. \end{aligned} \quad (71)$$

From the solution Eq. (72) we can obtain the particle density behaviour at large  $r$  and  $z$ , which are:

(i) for  $z \rightarrow \infty$ :

$$n \propto \frac{1}{z} \exp \left( -\frac{V_0}{\kappa_r} \frac{r}{z} \right), \quad (73)$$

(ii) and for  $r \rightarrow \infty$ :

$$n \propto \frac{1}{r} \exp \left( -\frac{V_0}{D_z} \frac{z}{r} \right). \quad (74)$$

From Eq. (54) it is clear that we are unable to describe the particle distribution near  $z = 0$  with the self-similar variable (Eq. (56)) and the function from Eq. (57), since it is impossible to satisfy the boundary conditions at  $\xi = \infty$ .

In order to study the radial behaviour of the distribution function near  $z = 0$  a different self-similar ansatz is used, which can be extended down to the spatial region near the sources. The similarity variable has the form

$$\hat{\xi} = \sqrt{\frac{\kappa_r}{D_z}} \frac{z}{r}, \quad (75)$$

and the transformed distribution function reads

$$\Phi(\hat{\xi}) = r^{-\mu} n(z, r). \quad (76)$$

Then Eq. (54) becomes

$$\begin{aligned} \left( \hat{\xi}^2 + 1 \right) \frac{d^2 \Phi}{d\hat{\xi}^2} + \left[ \left( 1 - 2\mu \right) \hat{\xi} - \frac{V_0}{\sqrt{D_z \kappa_r}} \right] \frac{d\Phi}{d\hat{\xi}} \\ + \mu^2 \Phi = -\frac{Q_0}{\kappa_r r^{\alpha + \mu - 2}} \delta(z), \end{aligned} \quad (77)$$

and if

$$\alpha + \mu - 2 = -1, \quad (78)$$

the RHS of Eq. (77) can also be cast into self-similar form

$$\frac{Q_0}{\kappa_r r^{\alpha + \mu - 2}} \delta(z) = \frac{Q_0}{\sqrt{D_z \kappa_r}} \delta(\hat{\xi}). \quad (79)$$

The boundary condition at  $\hat{\xi} = 0$  immediately follows from integration of Eq. (77) for small  $\hat{\xi}$ , in which case the equation becomes

$$\frac{d}{d\hat{\xi}} \left( \frac{d\Phi}{d\hat{\xi}} - \frac{V_0}{\sqrt{D_z \kappa_r}} \Phi \right) + \mu^2 \Phi = -\frac{Q_0}{\sqrt{D_z \kappa_r}} \delta(\hat{\xi}). \quad (80)$$

We integrate Eq. (80) along a box, encircling the Galactic plane with  $\hat{\xi} = 0$ , from  $-\varepsilon$  to  $+\varepsilon$ , and subsequently let  $\varepsilon \rightarrow 0$ . The formal integration near  $\hat{\xi} = 0$  gives the boundary condition at  $\hat{\xi} = 0$ ,

$$\frac{d\Phi(0)}{d\hat{\xi}} - \frac{V_0}{\sqrt{D_z \kappa_r}} \Phi(0) = -\frac{Q_0}{\sqrt{D_z \kappa_r}}. \quad (81)$$

The function  $\Phi$  is obtained by solving the homogeneous equation

$$\left( \hat{\xi}^2 + 1 \right) \frac{d^2 \Phi}{d\hat{\xi}^2} + \left[ (1 - 2\mu)\hat{\xi} - \frac{V_0}{\sqrt{D_z \kappa_r}} \right] \frac{d\Phi}{d\hat{\xi}} + \mu^2 \Phi = 0. \quad (82)$$

The solution of Eq. (82) is found to be

$$\begin{aligned} \Phi = & c_1 {}_2F_1 \left( -\mu, -\mu, 1 - \mu - \eta; \frac{1}{2} (1 \pm i\hat{\xi}) \right) \\ & + c_2 \left[ \frac{1}{2} (1 \pm i\hat{\xi}) \right]^{\eta + \mu} \\ & \times {}_2F_1 \left( \eta, \eta, 1 + \mu + \eta; \frac{1}{2} (1 \pm i\hat{\xi}) \right), \end{aligned} \quad (83)$$

where

$$\eta = \frac{1}{2} \left( 1 \mp \frac{iV_0}{\sqrt{D_z \kappa_r}} \right). \quad (84)$$

Our goal is to study the dependence of the particle density near  $z = 0$ , in other words we have to determine the value of  $\mu$ .

From the asymptotic expansion of hypergeometrical functions at  $\hat{\xi} \rightarrow \infty$ , we find that the solution Eq. (83) depends on  $\hat{\xi}$  as

$$\lim_{\hat{\xi} \rightarrow \infty} \Phi(\hat{\xi}) \propto \hat{\xi}^\mu. \quad (85)$$

This also follows directly from Eq. (77), which for large  $\hat{\xi}$  has the form

$$\hat{\xi}^2 \frac{d^2 \Phi}{d\hat{\xi}^2} + (1 - 2\mu)\hat{\xi} \frac{d\Phi}{d\hat{\xi}} + \mu^2 \Phi = 0. \quad (86)$$

It is easy to verify that  $\Phi$  behaves like a power law in  $\hat{\xi}$ , i.e.

$$\Phi \propto \hat{\xi}^\lambda \quad (87)$$

and the characteristic equation

$$\lambda(\lambda - 1) + \lambda(1 - 2\mu) + \mu^2 = 0 \quad (88)$$

has just one degenerate solution:

$$\lambda_{1,2} = \mu. \quad (89)$$

### Nucleon Distribution Function

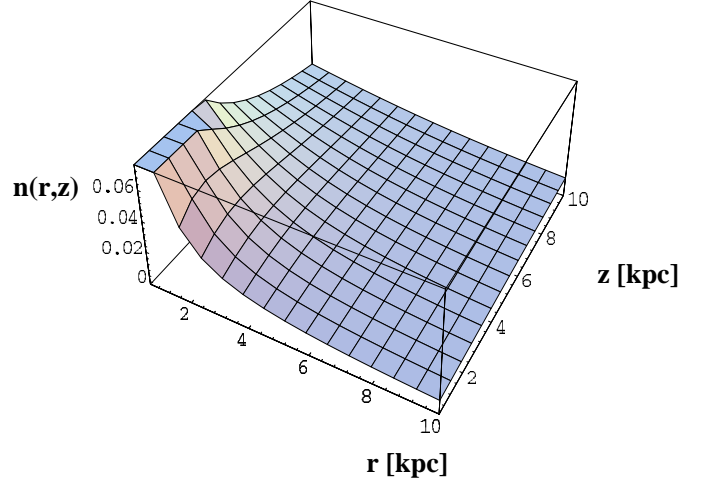


**Fig. 4.** The nucleon distribution function  $n(r, z)$  is plotted in arbitrary units as a function of Galactocentric radius  $r$  and height  $z$  above the plane. The radial and vertical diffusion coefficients are  $\kappa_r = 3 \times 10^{28} \text{ cm}^2 \text{ s}^{-1}$  and  $D_z = 3 \times 10^{28} \text{ cm}^2 \text{ s}^{-1}$ , respectively.

We have already shown that at large  $z$  the distribution function  $n$  has the form  $n \propto 1/z$  (cf. Eq. (73)). On the other hand it follows from Eq. (76) for  $\xi \rightarrow \infty$

$$n \propto r^\mu \Phi(\hat{\xi}) \propto r^\mu \hat{\xi}^\mu = z^\mu \quad (90)$$

and therefore  $\mu = -1$ , thus matching the two solutions obtained for different regions in  $r - z$ -space. It is clear that by the choice of the similarity variable (Eq. (75)), it is impossible to describe the distribution function near the Galactic centre ( $r \rightarrow 0$ ), but everywhere else in the disk.

Since close to the sources,  $\hat{\xi} \rightarrow 0$ ,  $\Phi \simeq \text{const.}$ , we derive from Eq. (76)

$$n(r) \propto \frac{1}{r}, \quad (91)$$

whereas the source distribution is required to have a radial exponent  $\alpha = 2$  as follows from Eq. (78), and therefore

$$Q(r) \propto \frac{1}{r^2}. \quad (92)$$

Thus radially dependent advection flattens the distribution of CRs in the disk as compared to the source distribution

$$f_2(r) \propto r^{-1}, \quad f_1(r) \propto r^{-2} \quad (93)$$

and the ‘‘compensation’’ condition, which in this case means a partial compensation since  $n \propto 1/r$  rather than  $n \sim \text{const.}$ , is realized in this case if

$$f_2^2 = f_1. \quad (94)$$

In Fig. 4 we have plotted the resulting nucleon distribution function, which shows a  $1/r$ -dependence (cf. Eq. (72)), thus flattening out the steeper radially dependent source distribution ( $\propto 1/r^2$ ) by a radially varying transition

### Nucleon distribution function

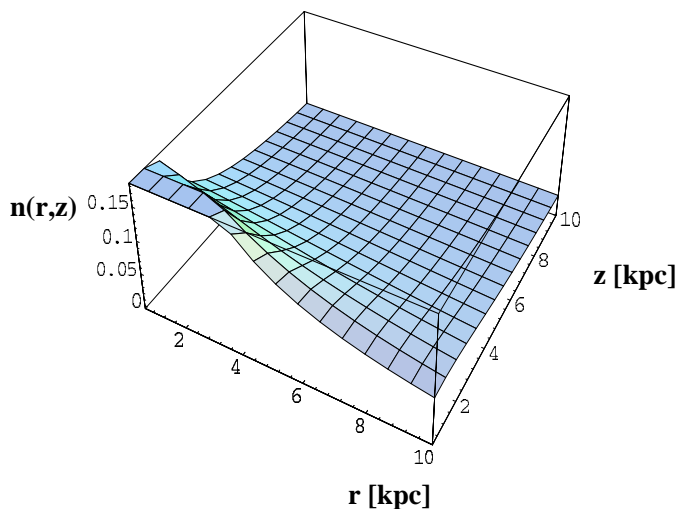


**Fig. 5.** Same as Fig. 4, but the radial and vertical diffusion coefficients are now different, viz.  $\kappa_r = 3 \times 10^{29} \text{ cm}^2 \text{ s}^{-1}$  and  $D_z = 3 \times 10^{28} \text{ cm}^2 \text{ s}^{-1}$ , respectively. This corresponds to *anisotropic* diffusion occurring preferentially in the *disk*, where the magnetic field is oriented mainly in radial direction.

### Nucleon distribution function

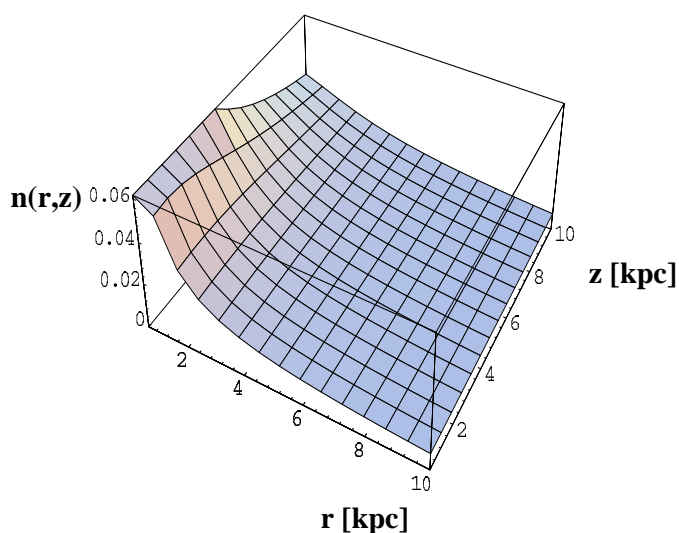


**Fig. 6.** Same as Fig. 5, with  $\kappa_r = 3 \times 10^{28} \text{ cm}^2 \text{ s}^{-1}$  and  $D_z = 3 \times 10^{29} \text{ cm}^2 \text{ s}^{-1}$ , respectively. This corresponds to *anisotropic* diffusion occurring preferentially in the *halo*, where the magnetic field is oriented mainly in the vertical direction.

boundary. It should be emphasized that such a behaviour is a natural consequence of the underlying radially varying source distribution itself. All previous models with  $z_C(r) = \text{const.}$  have ignored the growing influence of advective transport by an increase in CR sources and hence local CR pressure. Of course, it should be kept in mind that  $z_C$  is also energy dependent, since from observations of the CR spectrum it is inferred that  $D \propto E^\delta$ , where the value of  $\delta$  depends on  $z$ -variations of the Galactic wind velocity.

Moreover, according to Fig. 5, a stronger radial than vertical mixing of CRs due to *anisotropic* diffusion leads to a further flattening of the nucleon distribution function and hence to a weaker diffuse  $\gamma$ -ray gradient. We expect this to happen in the Galactic disk, where the geometry of the large scale magnetic field is mainly parallel to the disk. In contrast, in the halo a substantial vertical  $\mathbf{B}$ -component might exist (like e.g. in NGC 4631), resulting in a larger value of  $D_z$  as compared to  $\kappa_r$ . As can be seen from Fig. 6 this effect is competing to some extent with the also vertically directed advective velocity, and therefore the distribution function is similar to the one shown in Fig. 4.

In summary we conclude that the value of the halo extension calculated from the gradient data in the framework of the isotropic diffusion model may indeed be an artifact. In the next section we outline a general solution.

#### 8.4. General solution for axisymmetric convective and anisotropic diffusive CR transport

We now want to work out a general solution of the stationary two-dimensional CR transport equation for nucleons, without any restriction of the radial behavior of the source distribution  $Q(r, z)$ . In the following we use  $N(r, z, E)$  for the nucleon distribution function in order to avoid confusion with the number  $n$  for the enumeration of the poles in our solutions.

$$-\nabla \cdot (\underline{D}(\mathbf{x}, E) \nabla N - \mathbf{u}(\mathbf{x}) N) - \frac{\partial}{\partial E} \left( \frac{1}{3} \nabla \mathbf{u}(\mathbf{x}) \cdot E N \right) + \frac{\partial}{\partial E} \left( \frac{dE}{dt} N \right) = Q(E, \mathbf{x}), \quad (95)$$

where the diffusion tensor,  $\underline{D}$ , in cylindrical coordinates with axial symmetry is given by

$$\underline{D} = \begin{pmatrix} D_{rr} & D_{rz} \\ D_{rz} & D_{zz} \end{pmatrix} = \begin{pmatrix} \kappa_r & 0 \\ 0 & D_z \cdot E^\delta \end{pmatrix}. \quad (96)$$

We are not so much interested in energy dependent than spatially anisotropic diffusion and advection, and so, for convenience, we set  $\delta = 0$ . For the nucleon component other than adiabatic losses are negligible ( $dE/dt = 0$ ); thus Eq. (95) in axial symmetry reads

$$-D_z \frac{\partial^2 N}{\partial z^2} - \kappa_r \left( \frac{\partial^2 N}{\partial r^2} + \frac{1}{r} \frac{\partial N}{\partial r} \right) + 3 \frac{V_0}{r^2} \frac{\partial (N z)}{\partial z} - \frac{V_0}{r^2} \frac{\partial (N E)}{\partial E} = Q_1(r) \delta(z) E^{-\gamma_0}, \quad (97)$$

with

$$Q_1(r) = Q_0 f_1(r), \quad (98)$$

and where we have chosen a spatial variation for the velocity field as

$$\mathbf{u}(\mathbf{x}) = \begin{pmatrix} u_r \\ u_z \end{pmatrix} = \begin{pmatrix} 0 \\ 3 \frac{V_0}{r^2} z \end{pmatrix} = \begin{pmatrix} 0 \\ 3 V_0 f_2(r) z \end{pmatrix}, \quad (99)$$

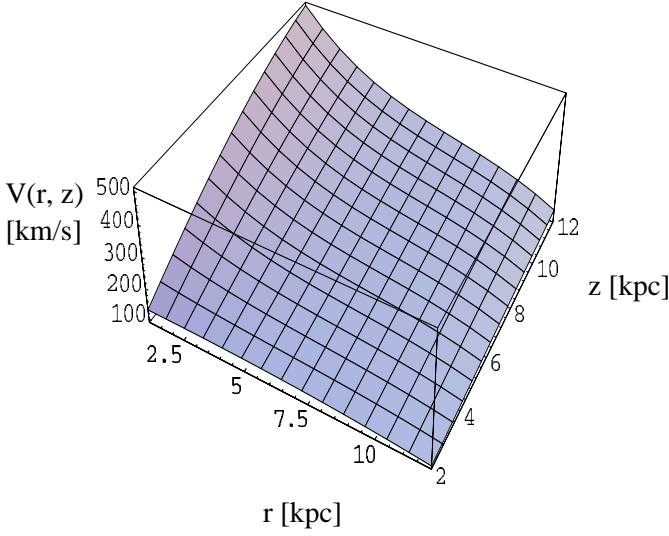


**Fig. 7.** Galactic wind outflow velocity ( $z$ -component),  $V(r, z) = u_z(r, z) + v_A(r, z)$ , as a function of Galactocentric radius  $r$  and vertical distance  $z$  from the Galactic plane, according to self-consistent Galactic wind calculations for a given SNR distribution (for details see text).

and a power law spectrum for injection by the disk sources. The choice of  $\mathbf{u}(\mathbf{x})$  is motivated not only by simplicity, but also by our numerical calculations (see Figs. 2 and 7). The latter figure shows the outflow velocity as observed in a fixed Galactic frame of reference,  $V(r, z) = u_z(r, z) + V_A(r, z)$ . It can be seen that  $V(r, z)$  increases roughly linearly with  $z$  and decreases in a power law fashion with  $r$ , so that Eq. (99) is a good first approximation. The boundary conditions for obtaining these results are given in Sect. 7. In future calculations, we will also test other analytical approximations to  $V(r, z)$ .

It is clear from Eq. (97) that the effect of anisotropic diffusion corresponds to stretching or compressing scales in respective directions, since in the new variables,  $\bar{r} = r/\sqrt{\kappa_r}$ , and,  $\bar{z} = z/\sqrt{D_z}$ , we recover the equation for isotropic diffusion. Obviously, this may also change the gradient of the cosmic ray density in the disk, but we will show that rather strong modifications of the density (including the observed uniform distribution of cosmic rays) can be obtained for spatially nonuniform advection.

In order to solve Eq. (97) analytically, we apply the following transformations

$$N(r, z, E) = E^{-\gamma_0} S(\xi, \varrho), \quad (100)$$

$$A = \frac{V_0}{\kappa_r}, \quad (101)$$

$$B = \sqrt{\frac{D_z}{\kappa_r}}, \quad (102)$$

$$\gamma = \gamma_0 + 2, \quad (103)$$

$$\bar{r} = Br, \quad (104)$$

$$\varrho = \ln \bar{r} \quad \implies \bar{r} = e^\varrho. \quad (105)$$

$$\xi = \frac{z}{\bar{r}} \quad \implies \xi = ze^{-\varrho}. \quad (106)$$

The differential operators for the variable transformation  $(r, z) \rightarrow (\varrho, \xi)$  are given by

$$\frac{\partial}{\partial r} = e^{-\varrho} \left( \frac{\partial}{\partial \varrho} - \xi \frac{\partial}{\partial \xi} \right), \quad (107)$$

$$\frac{\partial}{\partial z} = e^{-\varrho} \frac{\partial}{\partial \xi}, \quad (108)$$

$$\frac{\partial^2}{\partial r^2} = e^{-2\varrho} \left( \frac{\xi^2 \partial^2}{\partial \xi^2} - 2 \frac{\xi \partial^2}{\partial \xi \partial \varrho} + 2 \frac{\xi \partial}{\partial \xi} + \frac{\partial^2}{\partial \varrho^2} - \frac{\partial}{\partial \varrho} \right), \quad (109)$$

$$\frac{\partial^2}{\partial z^2} = e^{-2\varrho} \frac{\partial^2}{\partial \xi^2}. \quad (110)$$

Using the above transformations, Eq. (97) can be cast into

$$\begin{aligned} (1 + \xi^2) \frac{\partial^2 S}{\partial \xi^2} + \frac{\partial^2 S}{\partial \varrho^2} - 2\xi \frac{\partial^2 S}{\partial \xi \partial \varrho} + (1 - 3A) \xi \frac{\partial S}{\partial \xi} \\ - A \gamma S = - \frac{Q_1(e^\varrho)}{D_z} e^\varrho \delta(\xi). \end{aligned} \quad (111)$$

Next we transform the boundary conditions appropriately:

$$N(r, z = \pm\infty) = 0 \quad \longrightarrow \quad S(\varrho, \xi = \pm\infty) = 0 \quad (112)$$

$$N(r = +\infty, z) = 0 \quad \longrightarrow \quad S(\varrho = +\infty, \xi) = 0 \quad (113)$$

$$\frac{\partial N(r = 0, z)}{\partial r} = 0 \quad \longrightarrow \quad \left( e^{-\varrho} \frac{\partial S}{\partial \varrho} \right)_{\varrho=-\infty} = 0. \quad (114)$$

In order to proceed with the solution of Eq. (111), we look for the Green's function  $G(\xi, \varrho)$  of

$$\begin{aligned} (1 + \xi^2) \frac{\partial^2 G}{\partial \xi^2} + \frac{\partial^2 G}{\partial \varrho^2} - 2\xi \frac{\partial^2 G}{\partial \xi \partial \varrho} + (1 - 3A) \xi \frac{\partial G}{\partial \xi} \\ - A \gamma G = \delta(\varrho - \varrho') \delta(\xi). \end{aligned} \quad (115)$$

with boundary conditions

$$G(\varrho, \xi = \pm\infty) = 0, \quad (116)$$

$$G(\varrho = \pm\infty, \xi) = 0. \quad (117)$$

A standard method for solving PDE's of the above kind is to use integral transforms; since we consider a steady state problem over all  $r$ - and  $z$ -space (or  $\xi$  and  $\varrho$ , respectively) we use Fourier transforms of the kind

$$G(\xi, \varrho) = \int_{-\infty}^{+\infty} \frac{dk}{2\pi} F(k, \xi) \exp(-ik\varrho), \quad (118)$$

$$F(k, \xi) = \int_{-\infty}^{+\infty} G(\xi, \varrho) \exp(ik\varrho) d\varrho. \quad (119)$$

Inserting the transform Eq. (118) into Eq. (115), and after integrating by parts we apply the boundary conditions Eqs. (116)-(117) and end up with an ODE in  $\xi$ ,

$$\begin{aligned} (1 + \xi^2) F''(\xi) + (2ik - 3A + 1) \xi F'(\xi) \\ - (k^2 + A\gamma) F(\xi) = \delta(\xi) \exp(ik\varrho'). \end{aligned} \quad (120)$$

Let us inspect the associated homogeneous equation first. Eq. (120) can be cast into the hypergeometric differential equation

$$x(x-1)y'' + [(\alpha + \beta + 1)x - \tilde{\gamma}]y' + \alpha\beta y = 0, \quad (121)$$

by applying the following transformation

$$x = p + iq\xi \quad (122)$$

$$\Rightarrow dx = iq d\xi, \quad (123)$$

and

$$x(x-1) = p(p-1) - q^2\xi^2 + iq\xi(2p-1), \quad (124)$$

from which we infer  $p = 1/2$  and  $q = \pm 1/2$ . Matching the second term of Eq. (121) we obtain

$$\alpha + \beta + 1 = 1 - 3A + 2ik, \quad (125)$$

$$\tilde{\gamma} = \frac{1}{2}(\alpha + \beta + 1). \quad (126)$$

Note that there is no difference between the cases with “+” and “-”. The last term in Eq. (121) requires

$$\alpha\beta = -(k^2 + \gamma A). \quad (127)$$

Solving for  $\alpha$  and  $\beta$  from Eqs. (126) and (127) gives

$$\alpha_{1,2} = \frac{1}{2}(2ik - 3A \pm C), \quad (128)$$

$$\beta_{1,2} = \frac{1}{2}(2ik - 3A \mp C), \quad (129)$$

where  $C = \sqrt{A(9A - 12ik + 4\gamma)}$ . In Eqs. (128) and (129)  $\alpha$  and  $\beta$  are complementary and we can drop the subscripts, using “+” for  $\alpha$  and “-” for  $\beta$ .

Thus the solution of the homogeneous equation reads

$$\begin{aligned} F(\xi) = & c_1 {}_2F_1\left(\alpha, \beta, \tilde{\gamma}; \frac{1}{2}(1 \pm i\xi)\right) \\ & + c_2 \left[\frac{1}{2}(1 \pm i\xi)\right]^{1-\tilde{\gamma}} \\ & \times {}_2F_1\left(\alpha - \tilde{\gamma} + 1, \beta - \tilde{\gamma} + 1, 2 - \tilde{\gamma}; \frac{1}{2}(1 \pm i\xi)\right), \end{aligned} \quad (130)$$

where  $\tilde{\gamma}$  is not an integer and  $0 < \text{Re}(1 \pm i\xi) < 1$ .

Applying the linear transformation

$${}_2F_1(\alpha, \beta, \tilde{\gamma}; x) = (1-x)^{\tilde{\gamma}-\alpha-\beta} \times {}_2F_1(\tilde{\gamma}-\alpha, \tilde{\gamma}-\beta, \tilde{\gamma}; x), \quad (131)$$

we finally obtain

$$\begin{aligned} F(\xi) = & c_1 {}_2F_1\left(\alpha, \beta, \tilde{\gamma}; \frac{1}{2}(1 \pm i\xi)\right) \\ & + c_2 \left[\frac{1}{2}(1 \pm i\xi)\right]^{1-\tilde{\gamma}} \cdot \left[\frac{1}{2}(1 \mp i\xi)\right]^{\tilde{\gamma}-\alpha-\beta} \\ & \times {}_2F_1\left(1-\alpha, 1-\beta, 2-\tilde{\gamma}; \frac{1}{2}(1 \pm i\xi)\right), \\ = & c_1 {}_2F_1\left(\alpha, \beta, \tilde{\gamma}; \frac{1}{2}(1 \pm i\xi)\right) \\ & + c_2 \left[\frac{1}{4}(1 + \xi^2)\right]^{1-\tilde{\gamma}} \\ & \times {}_2F_1\left(1-\alpha, 1-\beta, 2-\tilde{\gamma}; \frac{1}{2}(1 \pm i\xi)\right), \end{aligned} \quad (132)$$

where the integration constants  $c_1$  and  $c_2$  have yet to be determined from the boundary conditions (see Appendix B). From the Fourier transforms (118) and (119) we see that this implies

$$F(\xi = \pm\infty) = 0; \quad (133)$$

furthermore we require

- (i) continuity of  $F(\xi)$  across  $\xi = 0$ ,
- (ii)  $F(-\xi) = F(\xi)$ .

We also note from Eq. (132) that  $F(\xi)$  is multivalued in the complex plane and therefore a branch cut has to be introduced, running along the imaginary axis from  $-i$  to  $+i$ .

We now return to the inhomogeneous equation (Eq. (120)). For  $\xi \neq 0$ , Eq. (132) is a valid solution; in order to evaluate the solution at  $\xi = 0$  we integrate Eq. (120) in the infinitesimal range  $-\varepsilon \leq \xi \leq \varepsilon$ , with  $|\varepsilon| \ll 1$  and then take the limit  $\varepsilon \rightarrow 0$ .

Exploiting the properties of the solution  $F(\xi)$  outlined above, and noting that the integration over an odd function vanishes, we obtain after a little algebra

$$F'(0^+) - F'(0^-) = \exp(ik\rho'), \quad (134)$$

which is a jump condition for the derivative at  $\xi = 0$ . Integrating this result over  $\xi$  gives

$$F(0^+) - F(0^-) = 0, \quad (135)$$

as expected. With Eqs. (133) and (134) we can now evaluate the constants  $c_1$  and  $c_2$  (see Eqs. (B.12) and (B.13), Appendix B).

Manipulating the  $\Gamma$ -functions with help of the relations in Appendix B (B.9–B.11) the solution for  $\xi = 0$  reads

$$\begin{aligned} F(0) = & \mp \frac{i \exp(ik\rho')}{2\pi^2} \left\{ \frac{\Gamma\left(\frac{\alpha}{2}\right) \Gamma\left(\frac{\beta}{2}\right) \Gamma\left(\frac{1-\alpha}{2}\right) \Gamma\left(\frac{1-\beta}{2}\right)}{(-1)^{\tilde{\gamma}} \sin\left(\frac{\pi\beta}{2}\right) + \cos\left(\frac{\pi\alpha}{2}\right)} \right. \\ & \left. \times \frac{\sin\left(\frac{\pi\beta}{2}\right) \cos\left(\frac{\pi\alpha}{2}\right) \left[(-1)^{\tilde{\gamma}} \cos\left(\frac{\pi\beta}{2}\right) + \sin\left(\frac{\pi\alpha}{2}\right)\right]}{(-1)^{\tilde{\gamma}} \sin\left(\frac{\pi\beta}{2}\right) + \cos\left(\frac{\pi\alpha}{2}\right)} \right\}. \end{aligned} \quad (136)$$

### 8.5. Solution in the disk

Using the solution for  $F(\xi = 0)$  we can now, as a special case, calculate the full solution in the disk, i.e.  $N(r, z = 0, E)$ . The Green's function is then given by Eq. (118)

$$G(\xi = 0, \varrho; \varrho') = \int_{-\infty}^{+\infty} \frac{dk}{2\pi} F(k, 0) \exp(-ik\rho'). \quad (137)$$

In our solution (136) we have suppressed the explicit dependence on  $k$ , but of course it is implicitly contained in  $\alpha(k)$ ,  $\beta(k)$ , and  $\tilde{\gamma}(k)$ .

Let  $K = ik$ , we obtain

$$G(0; \varrho, \varrho') = -\frac{i}{2\pi} \int_{-i\infty}^{+i\infty} \tilde{F}(K, 0) \exp[-K(\varrho - \varrho')] dK, \quad (138)$$

where  $\tilde{F}(K, 0) = \exp[-K \varrho'] F(K, 0)$ . Then

$$S(\xi, \varrho) = - \int_{-\infty}^{+\infty} G(\xi; \varrho, \varrho') \frac{Q_1(e^{\varrho'})}{D_z} e^{\varrho'} 2\pi e^{\varrho'} d\varrho'. \quad (139)$$

Transforming back to the variable  $\bar{r}$  and  $r'$  (Eq. (105)):

$$G(0; r, r') = \frac{-i}{2\pi} \int_{-i\infty}^{+i\infty} \tilde{F}(K, 0) \left(\frac{\bar{r}}{r'}\right)^{-K} dK, \quad (140)$$

and

$$S(\xi, r) = - \int_0^{+\infty} G(\xi; r, r') \frac{Q_1(r')}{D_z} 2\pi (r')^2 \frac{d\varrho'}{dr'} dr'. \quad (141)$$

The particle distribution in the disk is then given by

$$N(r, z=0, E) = \frac{-i}{2\pi D_z} E^{-\gamma_0} \times \int_0^{\infty} Q_1(r') 2\pi r' dr' \int_{-i\infty}^{+i\infty} \tilde{F}(K, 0) \left(\frac{\bar{r}}{r'}\right)^{-K} dK \quad (142)$$

and using the expression (136) for  $F(K, 0) = F(\xi = 0)$ , we obtain

$$N(r, z=0, E) = \mp \frac{1}{4\pi D_z} E^{-\gamma_0} \int_0^{\infty} Q_1(r') 2\pi r' dr' \times \int_{-i\infty}^{+i\infty} \frac{\Gamma\left(\frac{\alpha}{2}\right) \Gamma\left(\frac{1-\beta}{2}\right)}{\Gamma\left(\frac{1+\alpha}{2}\right) \Gamma\left(1-\frac{\beta}{2}\right)} \times \left\{ \frac{(-1)^{\tilde{\gamma}} \cos\left(\frac{\pi\beta}{2}\right) + \sin\left(\frac{\pi\alpha}{2}\right)}{(-1)^{\tilde{\gamma}} \sin\left(\frac{\pi\beta}{2}\right) + \cos\left(\frac{\pi\alpha}{2}\right)} \right\} \left(\frac{r}{r'}\right)^{-K} dK. \quad (143)$$

With the help of the Green's function from Appendix C (cf. Eqs. (C.10) and (C.11)) we obtain

$$N(r, z=0, E) = \mp \frac{1}{4\pi D_z} E^{-\gamma_0} \times \left\{ \int_r^{+\infty} Q_1(r') 2\pi r' dr' \int_{C_\alpha} \frac{\Gamma\left(\frac{\alpha}{2}\right) \Gamma\left(\frac{1-\beta}{2}\right)}{\Gamma\left(\frac{1+\alpha}{2}\right) \Gamma\left(1-\frac{\beta}{2}\right)} \times \left\{ \frac{(-1)^{\tilde{\gamma}} \cos\left(\frac{\pi\beta}{2}\right) + \sin\left(\frac{\pi\alpha}{2}\right)}{(-1)^{\tilde{\gamma}} \sin\left(\frac{\pi\beta}{2}\right) + \cos\left(\frac{\pi\alpha}{2}\right)} \right\} \left(\frac{\bar{r}}{r'}\right)^{-K} \frac{dK}{d\alpha} \right. \\ \left. + \int_0^r Q_1(r') 2\pi r' dr' \int_{C_\beta} \frac{\Gamma\left(\frac{\alpha}{2}\right) \Gamma\left(\frac{1-\beta}{2}\right)}{\Gamma\left(\frac{1+\alpha}{2}\right) \Gamma\left(1-\frac{\beta}{2}\right)} \times \left\{ \frac{(-1)^{\tilde{\gamma}} \cos\left(\frac{\pi\beta}{2}\right) + \sin\left(\frac{\pi\alpha}{2}\right)}{(-1)^{\tilde{\gamma}} \sin\left(\frac{\pi\beta}{2}\right) + \cos\left(\frac{\pi\alpha}{2}\right)} \right\} \left(\frac{\bar{r}}{r'}\right)^{-K} \frac{dK}{d\beta} d\beta \right\}, \quad (144)$$

where the integration contours  $C_\alpha$  and  $C_\beta$  correspond to  $r' > r$  and  $r' < r$ , respectively. The only poles to consider for  $A \gg 1$  are (see Fig. C.1) for  $n = 0, 1, 2, \dots$

$$\alpha(K_n) = -2n \implies K_n = -2n \pm \sqrt{A(\gamma + 6n)}, \quad (145)$$

where the sign “-” should be chosen for  $K_n$ . The poles  $\alpha(K_n)$  are inside the contour  $C_\alpha$  (see Appendix C).

Then we get from the theorem of residues (the residues of Gamma functions  $\Gamma(n)$  at  $n = 0, -1, -2, \dots$  are given by  $\frac{(-1)^n}{n!}$ )

$$N(r, z=0, E) = \mp \frac{1}{4\pi D_z} E^{-\gamma_0} \left\{ \int_{\bar{r}}^{+\infty} Q_1(r') 2\pi r' dr' \times \sum_{n=0}^{\infty} \frac{(-1)^n \Gamma\left(\frac{1-\beta_n}{2}\right)}{n! \Gamma\left(\frac{1-2n}{2}\right) \Gamma\left(1-\frac{\beta_n}{2}\right)} \times \left\{ \frac{(-1)^{\tilde{\gamma}_n} \cos\left(\frac{\pi\beta_n}{2}\right)}{(-1)^{\tilde{\gamma}_n} \sin\left(\frac{\pi\beta_n}{2}\right) + (-1)^n} \right\} \left(\frac{\bar{r}}{r'}\right)^{-K_n} \frac{dK_n}{d\alpha} \right\}. \quad (146)$$

Here

$$\beta_n = -2n - 3A - 2\sqrt{A(\gamma + 6n)} \quad (147)$$

$$\tilde{\gamma}_n = \frac{1}{2} \left( 1 - 4n - 3A - 2\sqrt{A(\gamma + 6n)} \right) \quad (148)$$

$$K_n = -2n - \sqrt{A(\gamma + 6n)} \quad (149)$$

$$\frac{dK_n}{d\alpha} = 1 + \frac{3A}{2\sqrt{A(\gamma + 6n)}}. \quad (150)$$

Although Eq. (146) looks rather awkward, the solution for  $A \gg 1$  exhibits simple asymptotic dependencies at different radii. If the CR sources occupy a limited volume of the disk, bounded by a radius  $a$ ,  $Q(r') = Q_0 r'^{-q} \Theta(a - r')$ , then for  $r > a$  the function  $N$  is zero, since the integral  $\int_r^{+\infty} = 0$ . This means that advection can remove particles from the plane  $z = 0$  so fast that none remain in the plane at radii  $r > a$  (see Appendix C).

Inside the source region ( $r \ll a$ ),  $N(r)$  can be written as

$$N(r) \propto r \sqrt{A\gamma} \int_r^{+\infty} r'^{(1-q-\sqrt{A\gamma})} dr, \quad (151)$$

so that for strong advection  $A \gg 1$  the integral is determined by the lower limit *independent* of the source distribution. Then we have

$$N(r) \propto r^{2-q}, \quad (152)$$

and the CR density is almost constant in the disk region if  $q \approx 2$ . We have therefore demonstrated that in the case of strong and spatially nonuniform advection, the CR density in the disk exhibits only a weak gradient in spite of strong radial variations of the source distribution. Such a behaviour may be responsible for the mild gradient observed in the diffuse  $\gamma$ -ray data.

In the diffusion dominated case ( $A \ll 1$ ) the values of the integrals are determined by the source distribution. Here we should take into account the integral over  $C_\beta$ , which is not zero (see Appendix C). Far away from the disk, i.e.  $r \gg a$ , the distribution function is determined by the only pole,  $\beta = 1$ , which is inside the contour  $C_\beta$

(see Fig. C.5). Therefore independent of the source distribution, we have

$$N(r) \propto r^{-1-\sqrt{A(\gamma-3)}} \propto r^{-1}, \quad (153)$$

just what is expected for pure diffusive particle propagation.

Therefore we conclude from these analyses that a more or less uniform CR distribution in the disk can be expected, if advection is strong, i.e.  $A \gg 1$ .

The ‘‘compensation’’ equation in this case reads

$$f_2(r) = f_1(r). \quad (154)$$

The interesting conclusion from the solution of the general three-dimensional model is that we can reach a quasi-uniform CR distribution especially when the boundary  $z_C$  is *closest* to the Galactic plane in regions where the source density and hence advection is strongest (see also Fig. 3), i.e. when  $A \gg 1$ . This is in sharp contrast to the results of the pure diffusion model, because only an extremely extended galactic halo can produce a more or less smooth CR distribution and thus a mild diffuse  $\gamma$ -ray gradient.

## 9. Source contributions to the $\gamma$ -ray background

The examples of the last section substantiate our argument that transport effects should be responsible for all but eliminating the  $\gamma$ -ray gradient in the GeV energy range. This ignores possible contributions to the  $\gamma$ -ray flux from the sources themselves. In fact, SNRs as CR sources are expected to accumulate the accelerated CRs before releasing them into the ISM at the end of their lifetime. In nuclear collisions with thermal gas atoms or (for electrons) with photons inside the remnant, this high density of energetic particles will produce a strong  $\gamma$ -ray intensity that contributes a ‘‘diffuse’’ background if these sources are unresolved. In fact the ensemble of Galactic SNRs, expected to be strongly concentrated in the disk, will constitute such a background with typically less than about 10 such sources along a line of sight in the disk. They will be unresolved in GeV  $\gamma$ -rays, except for a few well-known nearby objects (Berezhko & Völk 2000); also their collective flux contributes less than 10% to the overall  $\gamma$ -ray flux. However, we know that the CR source spectrum is much harder  $\propto E^{-(2.1 \text{ to } 2.2)}$  than the diffuse Galactic CR energy spectrum ( $\propto E^{-2.7}$ ), and therefore the source contribution will equal the truly diffuse  $\gamma$ -ray flux at about 100 GeV and become even dominant at about  $10^3$  GeV (= 1 TeV).

If the sources collectively dominate in the form of an unresolved ‘‘diffuse’’ background at very high  $\gamma$ -ray energies, then it should be possible to observe the average CR source distribution and even the average CR source spectrum (!) along the Galactic disk in the TeV range. Present observations at TeV energies have not yet been able to detect this ‘‘diffuse’’ background. However, the experimental upper limits and the predicted ‘‘diffuse’’ flux are so close to each other (Aharonian et al. 2001) that

an instrumental increase by an order of magnitude should lead to a detection. The next generation of TeV instruments like H.E.S.S., CANGAROO, MAGIC or Veritas, that has this sensitivity, will come on line soon. The comparison of such a detected TeV-distribution with the radial shape of the source distribution from radio studies would constitute a stringent empirical test on our theoretical arguments about the transport effects on the truly diffuse Galactic CR component. It also shows the basic importance of  $\gamma$ -ray surveys over a large range in energies and radial distance.

## 10. Discussion and conclusions

In the detailed analysis of the previous sections it was shown that a physically reasonable CR transport model should include the nonlinear dynamical effects of the Galactic distribution of the CR sources themselves. Taking into account a simple radial dependence of the source power as suggested by radio observations of supernova remnants and pulsars, and thus averaging over all azimuthal angles, leads already to a radically different spatial behaviour of the CR distribution function. In all cases we have studied so far, there is a clear tendency to smooth out peaks due to enhanced particle injection by the sources in the ensuing radial particle distribution. This can be attributed to *CR advection in an outflow* aided or even caused by the CRs themselves. In other words, the importance of CR advection is proportional to the CR power of the underlying sources. As a consequence, e.g. the CR escape time, which is usually inferred from secondary radioactive isotopes, need no longer be a globally averaged quantity, but could vary strongly from place to place in the Galaxy. Therefore, the usual assumption that parameters of the CR flux measured near Earth are representative for the global processes of CR propagation in the Galaxy may be a misleading oversimplification.

It is common practice to determine from the intensities of different CR components near Earth the average diffusion coefficient in the Galaxy, the velocity of advection, the height of the CR halo in the direction perpendicular to the Galactic plane, and the CR injection spectrum, just to name the most important ones. Based on this hypothesis the nearly uniform radial CR distribution, derived from the measurement of diffuse Galactic  $\gamma$ -rays, can be reproduced only if there exists thorough spatial mixing of CRs in the framework of an extended halo (if CR diffusion is isotropic). Hence in such a case *local* and *global* properties of CRs do not differ from each other. However, the inferred halo height from chemical composition ( $z_C = 2\text{--}4$  kpc; see e.g., Bloemen et al. 1991, 1993; Webber et al. 1993; Lukasiak et al. 1994) is clearly inconsistent with the value derived from the interpretation of the  $\gamma$ -ray data ( $z_C = 15\text{--}20$  kpc; cf. Dogiel & Uryson 1988; Bloemen et al. 1993) within the framework of an isotropic diffusion model (see Appendix A). We therefore conclude that the halo size derived from CR nuclear data reflects only a local value near Earth, and the huge halo

extension derived previously from  $\gamma$ -ray data may be an artifact, since it relies on the validity of global values for locally obtained CR data. This conclusion is supported by our numerical galactic wind simulations, which show that the vertical distance of the diffusion-advection transition boundary from the Galactic plane, is inversely proportional to the CR source power and not spatially constant as been previously assumed.

Radio observations of external galaxies indicate a large-scale magnetic field geometry, which is mainly parallel to the major axis in the disk, and if a halo field exists, it is parallel to the minor axis. Therefore we expect that CR diffusion is in general *anisotropic*, with a radial diffusion coefficient  $\kappa_r$  in the disk, which is much larger than diffusion in the perpendicular direction,  $D_z$ , and vice versa in the halo. In this case the initially inhomogeneous CR distribution, due to a radially varying source distribution in the disk, is smeared out, whereas in the halo the dominant diffusion component  $D_z$  can be superposed by a strong advection velocity, which may determine the spatial particle distribution.

It would be desirable to have a high enough spatial resolution and photon statistics in the future to observe the radial distribution of diffuse  $\gamma$ -rays above 100 MeV in nearby edge-on galaxies, such as NGC 253. However, it seems unlikely that both space-borne and ground-based  $\gamma$ -ray observatories will satisfy this requirement in the near future. Thus the only direct observation of the CR source distribution in the Galaxy will be possible with next generation TeV instruments like H.E.S.S.

*Acknowledgements.* DB acknowledges support from the Deutsche Forschungsgemeinschaft (DFG) by a Heisenberg fellowship. He thanks the Max-Planck-Institut für Kernphysik in Heidelberg, the Max-Planck-Institut für extraterrestrische Physik in Garching, and the Department of Astrophysical Sciences of Princeton University, where this research has been carried out, for support and hospitality. DB thanks Russell Kulsrud for many interesting discussions.

VAD acknowledges financial support from the Alexander von Humboldt-Stiftung which was very essential for these collaborative researches. This work was prepared during his visit to Max-Planck-Institut für extraterrestrische Physik (Garching) and he is grateful to his colleagues from this institute for helpful and fruitful discussions. The final version of the paper was partly done at the Institute of Space and Astronautical Science. VAD thanks his colleagues from the institute and especially Prof. H. Inoue for their warm hospitality.

## Appendix A: The halo size from local characteristics of the CR flux

The flux of CRs observed near Earth (locally) contains information about regions from where these high energy particles have been produced, as well as about the location of the boundary from where these particles escape into the intergalactic medium and do not return to the Galactic disk. This means that in principle we can infer the size of the diffusion region simply from local CR properties. Let us denote the thickness of this region by  $z_{\text{esc}}$ .

We will demonstrate how to derive this quantity from a set of simplified equations, describing densities of stable and radioactive secondary nuclei generated by primary CRs in the gaseous disk.

For a one-dimensional diffusion model the system of equations for the density of stable,  $n_s$ , and radioactive,  $n_r$ , nuclei is given by

$$D \frac{d^2 n_s}{dz^2} = -N_g v \sigma_{\text{sp}} z_d n_p^0 \delta(z), \quad (\text{A.1})$$

and

$$D \frac{d^2 n_r}{dz^2} - \frac{n_r}{\tau} = -N_g v \sigma_{\text{rp}} z_d n_p^0 \delta(z). \quad (\text{A.2})$$

The distribution function of the nuclei in the disk is not very sensitive to the boundary conditions. Therefore we analyze here the simplest case, in which at  $z_{\text{esc}}$  it is required that

$$n_s, n_r = 0; \quad (\text{A.3})$$

here  $\sigma_{\text{sp}}$  and  $\sigma_{\text{rp}}$  are the spallation cross sections of stable and radioactive isotopes, respectively. We assume that processes of nuclear spallations take place in the gaseous disk with half-thickness  $z_d$ , which is much less than the halo scale height  $z_{\text{esc}}$ .

Here  $z$  is the coordinate perpendicular to the Galactic plane; the gas is supposed to be concentrated in the Galactic disk with  $z_d \ll z_{\text{esc}}$ , where the gas density equals  $N_g$ , and  $n_p^0$  is the density of primary cosmic rays in the disk ( $z = 0$ ). Then

$$n_s = N_g v \sigma_{\text{sp}} n_p^0 \frac{z_d}{D} (z_{\text{esc}} - z), \quad (\text{A.4})$$

and correspondingly

$$n_r = N_g v \sigma_{\text{rp}} n_p^0 \frac{z_d \sqrt{D\tau}}{D} \frac{\sinh\left(\frac{z_{\text{esc}} - z}{\sqrt{D\tau}}\right)}{\cosh\left(\frac{z_{\text{esc}}}{\sqrt{D\tau}}\right)}, \quad (\text{A.5})$$

and thus the ratio  $\frac{n_s}{n_r}$  at  $z = 0$  is

$$f = \frac{n_r}{n_s} = \frac{\sigma_{\text{rp}}}{\sigma_{\text{rs}}} \frac{\sqrt{D\tau}}{z_h} \tanh \frac{z_{\text{esc}}}{\sqrt{D\tau}}. \quad (\text{A.6})$$

The CR life-time in the region of diffusion propagation is determined from

$$\tau_{\text{esc}} \sim \frac{z_{\text{esc}}^2}{D}, \quad (\text{A.7})$$

and for  $\tau \ll \tau_{\text{esc}}$  we obtain

$$f = \frac{n_r}{n_s} \simeq \frac{\sigma_{\text{rp}}}{\sigma_{\text{sp}}} \sqrt{\frac{\tau}{\tau_{\text{esc}}}} = \frac{\sigma_{\text{rp}}}{\sigma_{\text{sp}}} \frac{\sqrt{D\tau}}{z_{\text{esc}}}. \quad (\text{A.8})$$

We see that this ratio depends on the two unknown parameters  $D$  and  $z_{\text{esc}}$ . Therefore they cannot be determined independently. To eliminate one parameter, we need additional observational constraints, for instance the average

thickness of matter traversed by CR nuclei in the Galaxy during their lifetime, given by the expression

$$x = M_p N_g v \frac{z_d}{z_{\text{esc}}} \tau_{\text{esc}}, \quad (\text{A.9})$$

where  $v$  is the velocity of the nuclei and  $M_p$  is the proton rest mass.

Combining this with Eq. (A.8) we obtain

$$x \simeq \frac{M_p z_d N_g v \tau}{f^2 z_{\text{esc}}} \left( \frac{\sigma_{\text{rp}}}{\sigma_{\text{sp}}} \right)^2, \quad (\text{A.10})$$

which gives  $z_{\text{esc}} \simeq 1$  kpc, for  $z_d N_g \simeq 4 \times 10^{20} \text{ cm}^{-2}$ ,  $x \simeq 12\text{--}14 \text{ g cm}^{-2}$  (Ferrando et al. 1991; Ferrando 1993),  $\tau = 2.2 \times 10^6$  years and  $f \simeq 0.25$  (see e.g., Simpson & Garcia-Muñoz 1988). Here we took  $\sigma_{\text{rp}} \sim \sigma_{\text{sp}}$  for the estimate.

If we include the convection term into the kinetic equation the analysis becomes more complicated, but the result is almost the same. If the velocity depends on  $z$  as

$$V(z) = 3V_0 z, \quad (\text{A.11})$$

we obtain for the ratio  $f$  (see Bloemen et al. 1993)

$$f \simeq \sqrt{3V_0 \tau}, \quad (\text{A.12})$$

which requires  $V_0 \simeq 10 \text{ km s}^{-1} \text{ kpc}^{-1}$ . The grammage in this case is

$$x \sim M_p N_g v \frac{z_d z_{\text{esc}}}{D(E)}, \quad (\text{A.13})$$

where  $z_{\text{esc}}$  is the coordinate of the surface above the Galactic plane from where CRs are sucked away by the Galactic wind (i.e. the transition boundary between diffusion and advection).

$$z_{\text{esc}} \sim \sqrt{\frac{D(E)}{V_0}}. \quad (\text{A.14})$$

Combining Eqs. (A.12)–(A.13) we also obtain for ( $\sigma_{\text{rp}} \sim \sigma_{\text{sp}}$ )

$$x \simeq \frac{M_p z_d N_g v \tau}{f^2 z_{\text{esc}}} \quad (\text{A.15})$$

and  $z_{\text{esc}}$  is also about 1 kpc.

This value estimated from the chemical composition of CRs near Earth is usually defined as the size of the CR halo. On the other hand the halo size can be derived from the global  $\gamma$ -ray emissivity distribution in the Galactic plane. The value of  $z_{\text{esc}}$  then determines the size of the CR mixing volume, which is estimated to be at least 10 kpc. If the diffusion model would describe the CR distribution correctly and satisfactorily in the Galaxy, the estimates of  $z_{\text{esc}}$  obtained from *local* and *global* data would be similar. However, the sizes of the CR propagation region differ from each other by about one order of magnitude, ruling out pure diffusion as the sole CR transport process.

## Appendix B: Determination of the integration constants $c_1$ and $c_2$

Using the transformation formula

$$\begin{aligned} {}_2F_1(\alpha, \beta, \tilde{\gamma}; x) &= \frac{\Gamma(\tilde{\gamma})\Gamma(\beta - \alpha)}{\Gamma(\beta)\Gamma(\tilde{\gamma} - \alpha)} (-x)^{-\alpha} \\ &\times {}_2F_1\left(\alpha, 1 - \tilde{\gamma} + \alpha, 1 - \beta + \alpha; \frac{1}{x}\right) \\ &+ \frac{\Gamma(\tilde{\gamma})\Gamma(\alpha - \beta)}{\Gamma(\alpha)\Gamma(\tilde{\gamma} - \beta)} (-x)^{-\beta} \\ &\times {}_2F_1\left(\beta, 1 - \tilde{\gamma} + \beta, 1 - \alpha + \beta; \frac{1}{x}\right), \quad (\text{B.1}) \end{aligned}$$

observing that  $x = \frac{1}{2} \left(1 \pm \frac{i}{B} \xi\right)$ , and the limit (which of course will also hold upon interchanging  $\alpha$  and  $\beta$  due to their symmetry, see Eqs. (126) and (127))

$$\lim_{\xi \rightarrow \pm\infty} {}_2F_1\left(\alpha, 1 - \tilde{\gamma} + \alpha, 1 - \beta + \alpha; \frac{1}{\frac{1}{2} \left(1 \pm \frac{i}{B} \xi\right)}\right) = 1, \quad (\text{B.2})$$

we obtain from the condition (133) for Eq. (132) after some algebra

$$\begin{aligned} &\lim_{\xi \rightarrow \pm\infty} \left\{ e^{i\pi\alpha} \left[ \frac{1}{2} \left(1 \pm \frac{i}{B} \xi\right) \right]^{-\alpha} \right. \\ &\times {}_2F_1\left(\alpha, 1 - \tilde{\gamma} + \alpha, 1 - \beta + \alpha; \frac{1}{x}\right) \left[ c_1 \frac{\Gamma(\tilde{\gamma})\Gamma(\beta - \alpha)}{\Gamma(\beta)\Gamma(\tilde{\gamma} - \alpha)} \right. \\ &\left. \left. + c_2 e^{-i\pi(\tilde{\gamma}-1)} \frac{\Gamma(2 - \tilde{\gamma})\Gamma(\beta - \alpha)}{\Gamma(\beta - \tilde{\gamma} + 1)\Gamma(1 - \alpha)} \right] \right. \\ &\left. + e^{i\pi\beta} \left[ \frac{1}{2} \left(1 \pm \frac{i}{B} \xi\right) \right]^{-\beta} \right. \\ &\times {}_2F_1\left(\beta, 1 - \tilde{\gamma} + \beta, 1 - \alpha + \beta; \frac{1}{x}\right) \left[ c_1 \frac{\Gamma(\tilde{\gamma})\Gamma(\alpha - \beta)}{\Gamma(\alpha)\Gamma(\tilde{\gamma} - \beta)} \right. \\ &\left. \left. + c_2 e^{-i\pi(\tilde{\gamma}-1)} \frac{\Gamma(2 - \tilde{\gamma})\Gamma(\alpha - \beta)}{\Gamma(\alpha - \tilde{\gamma} + 1)\Gamma(1 - \beta)} \right] \right\} = 0. \quad (\text{B.3}) \end{aligned}$$

Observing that  $\text{Re}(\alpha) > 0$  and  $\text{Re}(\beta) < 0$ , Eq. (B.3) can only be satisfied in general, if

$$c_1 = (-1)^{\tilde{\gamma}} \frac{\Gamma(2 - \tilde{\gamma})\Gamma(\alpha)}{\Gamma(\tilde{\gamma})\Gamma(1 - \beta)} c_2. \quad (\text{B.4})$$

Next we use condition (134) to fix  $c_1$  and  $c_2$ . Making use of the relations

$$\begin{aligned} \frac{d}{dx} {}_2F_1(\alpha, \beta, \tilde{\gamma}; x) &= \\ \frac{\alpha\beta}{\tilde{\gamma}} {}_2F_1(\alpha + 1, \beta + 1, \tilde{\gamma} + 1; x), \quad & (\text{B.5}) \end{aligned}$$

$${}_2F_1\left(\alpha + 1, \beta + 1, \tilde{\gamma} + 1; \frac{1}{2}\right) = \frac{4\sqrt{\pi}\tilde{\gamma}}{\alpha\beta} \frac{\Gamma(\tilde{\gamma})}{\Gamma(\frac{\alpha}{2})\Gamma(\frac{\beta}{2})}, \quad (\text{B.6})$$

$$\begin{aligned} &{}_2F_1\left(2 - \alpha, 2 - \beta, 3 - \tilde{\gamma}; \frac{1}{2}\right) \\ &= \frac{4\sqrt{\pi}\Gamma(3 - \tilde{\gamma})}{(1 - \alpha)(1 - \beta)\Gamma(\frac{1 - \alpha}{2})\Gamma(\frac{1 - \beta}{2})}, \quad (\text{B.7}) \end{aligned}$$

we obtain

$$\begin{aligned} \lim_{\xi \rightarrow 0} F'(\xi) &= \exp(ik\rho') \\ &= \pm 4\pi \frac{i}{2B} \left\{ c_1 \frac{\Gamma(\tilde{\gamma})}{\Gamma\left(\frac{\alpha}{2}\right)\Gamma\left(\frac{\beta}{2}\right)} \right. \\ &\quad \left. + c_2 4^{\tilde{\gamma}-1} \frac{\Gamma(2-\tilde{\gamma})}{\Gamma\left(\frac{1-\alpha}{2}\right)\Gamma\left(\frac{1-\beta}{2}\right)} \right\}. \end{aligned} \quad (\text{B.8})$$

Inserting Eq. (B.4) into Eq. (B.8) we end up after some tedious algebra and using the following relations

$$\Gamma(1+z) = z\Gamma(z) \quad (\text{B.9})$$

$$\Gamma(z)\Gamma(1-z) = \frac{\pi}{\sin(\pi z)} \quad (\text{B.10})$$

$$\Gamma(2z) = \frac{1}{\sqrt{\pi}} 2^{2z-1} \Gamma(z)\Gamma\left(z + \frac{1}{2}\right), \quad (\text{B.11})$$

with

$$c_1 = \mp \frac{iB \exp(ik\rho')}{2\sqrt{\pi}} \frac{(-1)^{\tilde{\gamma}} \Gamma\left(\frac{\alpha}{2}\right)\Gamma\left(\frac{\beta}{2}\right)\sin\left(\frac{\pi\beta}{2}\right)}{\Gamma(\tilde{\gamma}) \left[ (-1)^{\tilde{\gamma}} \sin\left(\frac{\pi\beta}{2}\right) + \cos\left(\frac{\pi\alpha}{2}\right) \right]}, \quad (\text{B.12})$$

and

$$\begin{aligned} c_2 &= \mp \frac{iB \exp(ik\rho')}{\sqrt{\pi}} \\ &\quad \times \frac{2^{-(\alpha+\beta)} \cos\left(\frac{\pi\alpha}{2}\right)\Gamma\left(\frac{1-\alpha}{2}\right)\Gamma\left(\frac{1-\beta}{2}\right)}{\Gamma(2-\tilde{\gamma}) \left[ (-1)^{\tilde{\gamma}} \sin\left(\frac{\pi\beta}{2}\right) + \cos\left(\frac{\pi\alpha}{2}\right) \right]}. \end{aligned} \quad (\text{B.13})$$

### Appendix C: Determination of integration contours for the Green's function $G(\xi, \bar{r}, r')$

The Fourier transform

$$F(k, \xi) = \int_{-\infty}^{+\infty} G(\xi, \varrho) \exp(ik\varrho) d\varrho, \quad (\text{C.1})$$

of the Green's function of Eq. (115) is shown in Eq. (119) with the constants  $c_1$  and  $c_2$  taken from Eqs. (B.12) and (B.13). For the special case of the solution in the Galactic plane ( $\xi = 0$ ) Eq. (132) becomes

$$\begin{aligned} F(\xi = 0) &= \mp \frac{i \exp(ik\rho')}{2} \left\{ \frac{\Gamma\left(\frac{\alpha}{2}\right)\Gamma\left(\frac{1-\beta}{2}\right)}{\Gamma\left(\frac{1+\alpha}{2}\right)\Gamma\left(1-\frac{\beta}{2}\right)} \right. \\ &\quad \left. \times \frac{\left[ (-1)^{\tilde{\gamma}} \cos\left(\frac{\pi\beta}{2}\right) + \sin\left(\frac{\pi\alpha}{2}\right) \right]}{\left[ (-1)^{\tilde{\gamma}} \sin\left(\frac{\pi\beta}{2}\right) + \cos\left(\frac{\pi\alpha}{2}\right) \right]} \right\}. \end{aligned} \quad (\text{C.2})$$

Then the Green's function for  $\xi = 0$  reads

$$G(\xi = 0, \varrho) = \int_{-\infty}^{+\infty} \frac{dk}{2\pi} F(k, \xi = 0) \exp(-ik\varrho).$$

If  $K = ik$ , then the transform for the variable  $r$  is

$$G(0; \bar{r}, r') = \frac{-i}{2\pi} \int_{-i\infty}^{+i\infty} \tilde{F}(K, 0) \left(\frac{\bar{r}}{r'}\right)^{-K} dK, \quad (\text{C.3})$$

which is determined by the residues of the poles of the  $\Gamma$ -functions

$$\alpha(K_n) = -2n \quad (\text{C.4})$$

and

$$\beta(K_m) = 2m + 1, \quad (\text{C.5})$$

and by the residues of the poles determined from

$$(-1)^{\tilde{\gamma}} \sin\left(\frac{\pi\beta}{2}\right) + \cos\left(\frac{\pi\alpha}{2}\right) = 0. \quad (\text{C.6})$$

Since  $\tilde{\gamma} = \alpha + \beta + 1$  this equation can be written in the form

$$\begin{aligned} &\exp\left[i\pi\left(\alpha + \frac{\beta}{2} - \frac{1}{2}\right)\right] - \exp\left[i\pi\left(\alpha - \frac{\beta}{2} - \frac{1}{2}\right)\right] \\ &\quad + \exp\left[i\pi\left(-\beta - 1 + \frac{\alpha}{2}\right)\right] + \exp\left[i\pi\left(-\beta - 1 - \frac{\alpha}{2}\right)\right] \\ &= 0, \end{aligned} \quad (\text{C.7})$$

yielding

$$\beta = -\alpha - 1 + 4n. \quad (\text{C.8})$$

However, these values of  $\beta$  also make the numerator vanish, i.e.

$$(-1)^{\tilde{\gamma}} \cos\left(\frac{\pi\beta}{2}\right) + \sin\left(\frac{\pi\alpha}{2}\right) = 0, \quad (\text{C.9})$$

because all we are doing is to interchange  $\alpha$  and  $\beta$ . Thus  $\beta = -\alpha - 1 + 4n$  does not give any poles.

We see from Eq. (C.3) that the contour of integration should be enclosed in the semiplane  $\text{Re}(K > 0)$  for  $\bar{r} > r'$ , i.e. the contour  $C_\alpha$  in Figs. C.1 and C.2. In this case the integration over the outer part of the closed contour is zero and the function  $G$  equals the residues of the sum inside the closed contour only. For  $\bar{r} < r'$  the contour is enclosed in the outer part of the semiplane  $\text{Re}(K < 0)$ , i.e. the contour  $C_\beta$  in Figs. C.1 and C.2. The locations of the poles in the  $K$ -plane are determined from a one-to-one map of the contours onto the  $\alpha$ - and  $\beta$ -planes and subsequently Eqs. (C.4) and (C.5) are applied.

The Green's function reads

$$\begin{aligned} G(\xi = 0; r, r') &= \frac{-i}{2\pi} \left\{ \Theta(r' - r) \int_{C_\alpha} \tilde{F}(K_\alpha, \xi) \left(\frac{\bar{r}}{r'}\right)^{-K_\alpha} \right. \\ &\quad \times \frac{dK_\alpha}{d\alpha} d\alpha + \Theta(r - r') \int_{C_\beta} \tilde{F}(K_\beta, \xi) \left(\frac{\bar{r}}{r'}\right)^{-K_\beta} \\ &\quad \left. \times \frac{dK_\beta}{d\beta} d\beta \right\}, \end{aligned} \quad (\text{C.10})$$

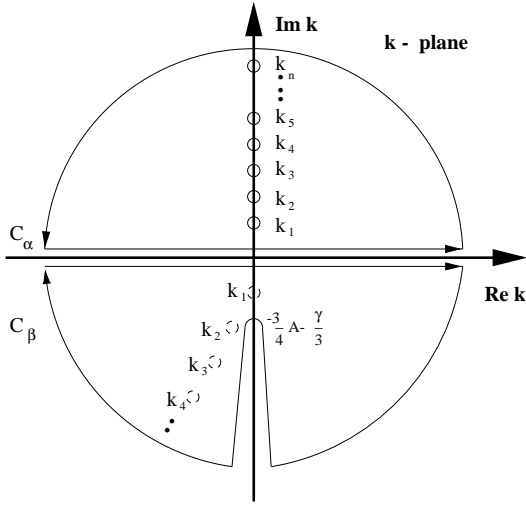


**Fig. C.1.** The contours of integration  $C_\alpha$  and  $C_\beta$  in Eq. (C.10) for  $\bar{r} < r'$  and  $\bar{r} > r'$  in the  $k$ -plane for  $A \gg 1$ . To show these contours in the  $K = ik$  plane the figure should be rotated by an angle of  $\pi/2$ . The dashed circles represent poles of the second kind, the solid circles poles of the first kind (see text).

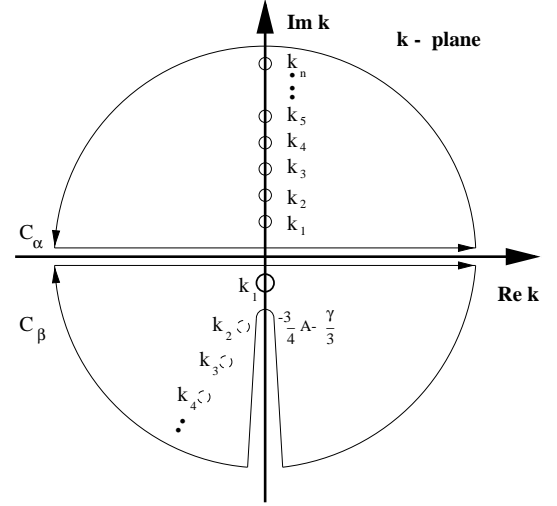


**Fig. C.2.** The contours of integration  $C_\alpha$  and  $C_\beta$  in Eq. (C.10) for  $\bar{r} < r'$  and  $\bar{r} > r'$  in the  $k$ -plane for  $A \ll 1$ . To show these contours in the  $K = ik$  plane the figure should be rotated by an angle of  $\pi/2$ . The dashed circles represent poles of the second kind, the solid circles poles of the first kind (see text).

and applying the theorem of residues we obtain

$$\begin{aligned}
 G(\xi = 0, r, r') = & \\
 & \frac{-i}{2\pi} \left\{ \Theta(r' - r) \left[ \sum \text{Res} \left( \Gamma \left( \frac{\alpha}{2} \right) \right) \right] \frac{\Gamma \left( \frac{1-\beta}{2} \right)}{\Gamma \left( \frac{1+\alpha}{2} \right) \Gamma \left( 1 - \frac{\beta}{2} \right)} \right. \\
 & \times \left\{ \frac{(-1)^{\tilde{\gamma}} \cos \left( \frac{\pi\beta}{2} \right) + \sin \left( \frac{\pi\alpha}{2} \right)}{(-1)^{\tilde{\gamma}} \sin \left( \frac{\pi\beta}{2} \right) + \cos \left( \frac{\pi\alpha}{2} \right)} \right\} \left( \frac{r}{r'} \right)^{-K} \\
 & + \Theta(r' - r) \left[ \sum \text{Res} \left( \Gamma \left( \frac{1-\beta}{2} \right) \right) \right] \frac{\Gamma \left( \frac{\alpha}{2} \right)}{\Gamma \left( \frac{1+\alpha}{2} \right) \Gamma \left( 1 - \frac{\beta}{2} \right)} \\
 & \times \left\{ \frac{(-1)^{\tilde{\gamma}} \cos \left( \frac{\pi\beta}{2} \right) + \sin \left( \frac{\pi\alpha}{2} \right)}{(-1)^{\tilde{\gamma}} \sin \left( \frac{\pi\beta}{2} \right) + \cos \left( \frac{\pi\alpha}{2} \right)} \right\} \left( \frac{r}{r'} \right)^{-K} \left. \right\}, \quad (\text{C.11})
 \end{aligned}$$

where  $\alpha, \beta, \tilde{\gamma}$  and  $K$  are determined by their values at the poles of the Gamma functions. The residues of the function  $\Gamma(n)$  have the value  $\frac{(-1)^n}{n!}$  at  $n = 0, -1, -2, \dots$

The contours for  $\bar{r} > r'$  and  $\bar{r} < r'$  in the  $k$ -plane are shown for  $A \gg 1$  in Fig. C.1, and for  $A \ll 1$  in Fig. C.2.

To determine the locations of the poles of the  $\Gamma$ -functions  $\alpha(K_n)$  and  $\beta(K_m)$  in the  $K$ -plane we should map a unique array of  $K$  values one-to-one onto corresponding arrays of  $\alpha$  and  $\beta$  values. In this way we define the contours of  $\text{Re}(K) > 0$  and  $\text{Re}(K) < 0$  in  $\alpha$  and  $\beta$  planes.

We start with  $r > r'$ . We find from  $\alpha(K = 0)$  (see Fig. C.3) that the contour  $C_\alpha$  intersects the abscissa at the points:

$$-\infty \quad \text{and} \quad -\frac{3A}{2} + \frac{1}{2}\sqrt{A(9A + 4\gamma)}. \quad (\text{C.12})$$

Therefore all poles  $\alpha_n$  are inside the contour  $C_\alpha$ . On the other hand the area encircled by  $C_\alpha$  does not contain

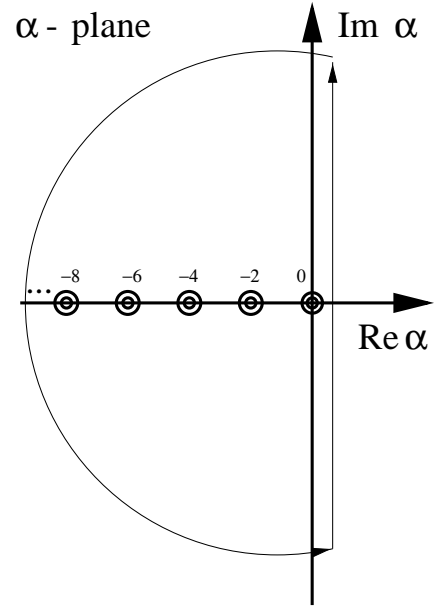


**Fig. C.3.** The contour of integration  $C_\alpha$  for  $\bar{r} < r'$  in the  $\alpha$ -plane. The solid circles represent poles inside the contour  $C_\alpha$ .

poles  $\beta_m$ . We see that poles  $\alpha_n$  mapped onto the  $k$ -plane are transformed to the negative part of the real axis (see Figs. C.1–C.3).

Since there is a branch point in the  $k$ -plane at

$$k = -i \left( \frac{3A}{4} + \frac{\gamma}{3} \right) \quad (\text{C.13})$$

the contour of integration  $C_\beta$  ( $r > r'$ ) has a cut (see Figs. C.1 and C.2). Its reflection in the  $\beta$ -plane is shown in Figs. C.4 and C.5. We see that the contour  $C_\beta$  intersects the abscissa at the points

$$-\frac{3A}{2} - \frac{1}{2}\sqrt{A(9A + 4\gamma)} \quad (\text{C.14})$$

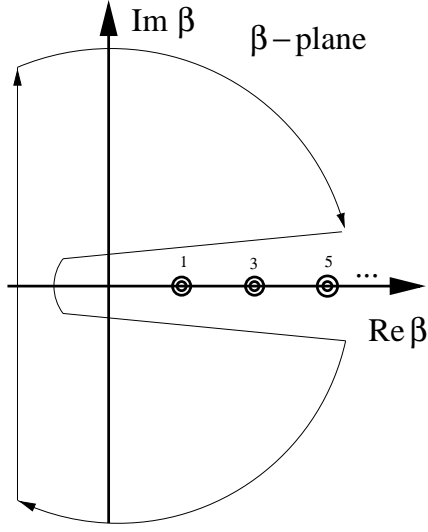


**Fig. C.4.** The contour of integration  $C_\beta$  and the poles  $\beta_m$  for  $\bar{r} > r'$  in the  $\beta$ -plane for  $A \gg 1$ .

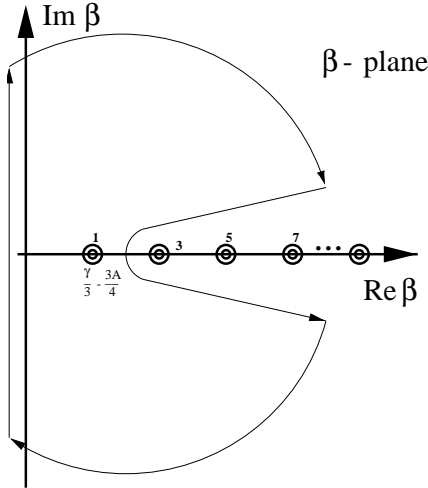


**Fig. C.5.** The contour of integration  $C_\beta$  for  $\bar{r} > r'$  in the  $\beta$ -plane for  $A \ll 1$ .

and

$$-\frac{3A}{4} + \frac{\gamma}{3}. \quad (\text{C.15})$$

The value of the latter is negative for  $A \gg 1$  and positive for  $A \ll 1$  ( $\gamma \simeq 4$ ). Therefore only if  $A \ll 1$  the pole  $\beta = 1$  is inside the contour  $C_\beta$  (see Fig. C.5). Correspondingly, there is only one pole inside the contour  $C_\beta$  in the  $k$ -plane (cf. Fig. C.2). In the opposite case,  $A \gg 1$ , all poles are outside this area (see Fig. C.4) and then the integral over  $C_\beta$  equals zero. This means that the poles  $\beta_m$  mapped onto the  $k$ -plane are of the second kind (their phases are larger than  $2\pi$ , see Fig. C.1). The reason, is that in the case of strong advection and the velocity increasing towards the center as  $r^{-2}$ , advection removes cosmic rays from the central part of the disk so fast that these particles do not reach its outer parts. Therefore the contribution of the integral over  $C_\beta$  (the central part of the disk) is zero and

the Green's function is determined by the integral over  $C_\alpha$  only.

We conclude this section by deriving the transformations between  $K$ -,  $\alpha$ - and  $\beta$ -planes, and by deriving the Green's functions both for strong and weak advection. From the condition of one-to-one correspondence we obtain for the poles in the  $K$ -plane

$$\alpha(K_n) = -2n \implies K_n = -2n - \sqrt{A(\gamma + 6n)}. \quad (\text{C.16})$$

$$\beta(K_m) = 2m + 1 \implies K_m = 2m + 1 + \sqrt{A(\gamma - 3(2m + 1))}. \quad (\text{C.17})$$

Since

$$\alpha(K_n) = -2n \quad (\text{C.18})$$

$$\beta(K_m) = 2m + 1, \quad (\text{C.19})$$

for  $n, m = 0, 1, 2, \dots$  we have

$$\beta_n = -2n - 3A - 2\sqrt{A(\gamma + 6n)} \quad (\text{C.20})$$

$$\tilde{\gamma}_n = \frac{1}{2} \left( 1 - 4n - 3A - 2\sqrt{A(\gamma + 6n)} \right) \quad (\text{C.21})$$

$$K_n = -2n - \sqrt{A(\gamma + 6n)} \quad (\text{C.22})$$

$$\frac{dK_n}{d\alpha} = 1 + \frac{3A}{2\sqrt{A(\gamma + 6n)}} \quad (\text{C.23})$$

$$\alpha_m = 2m + 1 - 3A + 2\sqrt{A(\gamma - 3(2m + 1))} \quad (\text{C.24})$$

$$\tilde{\gamma}_m = \frac{1}{2} \left( 2(2m + 1) - 3A + 1 + 2\sqrt{A(\gamma - 3(2m + 1))} \right) \quad (\text{C.25})$$

$$K_m = 2m + 1 + \sqrt{A(\gamma - 3(2m + 1))} \quad (\text{C.26})$$

$$\frac{dK_m}{d\beta} = 1 - \frac{3A}{2\sqrt{A(\gamma - 3(2m + 1))}} \quad (\text{C.27})$$

and for  $A \gg 1$  (cf. Eq. (C.10)):

$$G(\xi = 0, r, r') =$$

$$\begin{aligned} & \frac{-i}{2\pi} \left\{ \Theta(r' - r) \sum_{n=0}^{\infty} \frac{(-1)^n \Gamma\left(\frac{1-\beta_n}{2}\right)}{n! \Gamma\left(\frac{1-2n}{2}\right) \Gamma\left(1 - \frac{\beta_n}{2}\right)} \right. \\ & \times \left. \left\{ \frac{(-1)^{\tilde{\gamma}_n} \cos\left(\frac{\pi\beta_n}{2}\right)}{(-1)^{\tilde{\gamma}_n} \sin\left(\frac{\pi\beta_n}{2}\right) + (-1)^n} \right\} \left(\frac{\bar{r}}{r'}\right)^{-K_n} \frac{dK_n}{d\alpha} \right\}. \quad (\text{C.28}) \end{aligned}$$

For  $A \ll 1$  the Green's function reads

$$G(\xi = 0, r, r') =$$

$$\begin{aligned} & \frac{-i}{2\pi} \left\{ \Theta(r' - r) \sum_{n=0}^{\infty} \frac{(-1)^n \Gamma\left(\frac{1-\beta_n}{2}\right)}{n! \Gamma\left(\frac{1-2n}{2}\right) \Gamma\left(1 - \frac{\beta_n}{2}\right)} \right. \\ & \times \left\{ \frac{(-1)^{\tilde{\gamma}_n} \cos\left(\frac{\pi\beta_n}{2}\right)}{(-1)^{\tilde{\gamma}_n} \sin\left(\frac{\pi\beta_n}{2}\right) + (-1)^n} \right\} \left(\frac{\bar{r}}{r'}\right)^{-K_n} \frac{dK_n}{d\alpha} \\ & + \Theta(r - r') \frac{\Gamma\left(\frac{\alpha_\beta}{2}\right)}{\Gamma\left(\frac{1}{2}\right) \Gamma\left(1 + \frac{\alpha_\beta}{2}\right)} \\ & \times \left. \left\{ \frac{\sin\left(\frac{\pi\alpha_\beta}{2}\right)}{(-1)^{\tilde{\gamma}_\beta} + \cos\left(\frac{\pi\alpha_\beta}{2}\right)} \right\} \left(\frac{\bar{r}}{r'}\right)^{-K_\beta} \frac{dK_\beta}{d\beta} \right\}, \quad (\text{C.29}) \end{aligned}$$

where

$$\beta = 1 \quad (\text{C.30})$$

$$\alpha_\beta = 1 - 3A + 2\sqrt{A(\gamma - 3)} \quad (\text{C.31})$$

$$\tilde{\gamma}_\beta = \frac{1}{2} \left( 2 - 3A + 1 + 2\sqrt{A(\gamma - 3)} \right) \quad (\text{C.32})$$

$$K_\beta = 1 + \sqrt{A(\gamma - 3)} \quad (\text{C.33})$$

$$\frac{dK_m}{d\beta} = 1 - \frac{3A}{2\sqrt{A(\gamma - 3)}}. \quad (\text{C.34})$$

## References

- Aharonian, F. A., et al. 2001, *A&A*, submitted
- Aharonian, F. A., & Atoyan, A. M. 1999, *A&A*, 362, 937
- Axford, W.I., Leer, E., & Skadron, G. 1977, in Proceedings of 15th Int. Cosmic Ray Conf. (Plovdiv), Bulg. Acad. Sci., 2, 273
- Bakhareva, M. V., & Smirnova, V. V. 1980, *Geomagn. Aeron.*, 20, 5
- Bell, A. R. 1978a, *MNRAS*, 182, 147
- Bell, A. R. 1978b, *MNRAS*, 182, 443
- Berezhko, E. G., Yelshin, V. K., & Ksenofontov, L. T. 1994, *APh*, 2, 215
- Berezhko, E. G., & Völk, H. J. 2000, *ApJ*, 540, 923
- Berezinsky, V. S., Bulanov, S. V., Dogiel, V. A., Ginzburg, V. L., & Ptuskin, V. S. 1990, *Astrophysics of Cosmic Rays*, ed. V. L. Ginzburg (North Holland)
- Blandford, R. D., & Ostriker, J. P. 1978, *ApJ*, 221, L29
- Bloemen, J. B. G. M., Dogiel, V. A., Dorman, V. L., & Ptuskin, V. S. 1991, *Izv.AN SSSR, Ser. fizich.*, 55, 2052
- Bloemen, J. B. G. M., Dogiel, V. A., Dorman, V. L., & Ptuskin, V. S. 1993, *A&A*, 267, 372
- Breitschwerdt, D. 1994, *Habilitation-Thesis* (University Heidelberg), 158
- Breitschwerdt, D., McKenzie, J. F., & Völk, H. J. 1987, in *Interstellar Magnetic Fields*, ed. R. Beck, & R. Gräve (Springer), 131
- Breitschwerdt, D., McKenzie, J. F., & Völk, H. J. 1991, *A&A*, 245, 79
- Breitschwerdt, D., McKenzie, J. F., & Völk, H. J. 1993, *A&A*, 269, 54
- Breitschwerdt, D., & Schmutzler, T. 1994, *Nature*, 371, 774
- Breitschwerdt, D., & Schmutzler, T. 1999, *A&A*, 347, 650
- Bykov, A. M., & Fleishman, G. D. 1992, *MNRAS*, 255, 269
- Case, G. L., & Bhattacharya, D. 1996, *AAS*, 120, 437
- Case, G. L., & Bhattacharya, D. 1998, *ApJ*, 504, 761
- Dettmar, R.-J. 1992, *Fund. Cos. Phys.*, 15, 143
- Digel, S. W., Grenier, I. A., Heithausen, A., Hunter, S. D., & Thaddeus, P. 1996, *ApJ*, 463, 609
- Dogiel, V. A., & Schönfelder, V. 1997, in *Radiophys. Quant. Electron.*, 40, 57
- Dogiel, V. A., & Uryson, A. V. 1988, *A&A*, 197, 335
- Dogiel, V. A., Gurevich, A. V., & Zybin, K. P. 1994, *A&A*, 281, 937
- Dragicevich, P. M., Blair, D. G., & Burman, R. R. 1999, *MNRAS*, 302, 693
- Drury, L. O'C., Markiewicz, W. J., & Völk, H. J. 1989, *A&A*, 225, 179
- Erlykin, A. D., Fatemi, S. J., Wolfendale, A. W., & Zhang, L. 1996, *A&AS*, 120, 415
- Evans, R., van den Bergh, & S., McClure, R. D. 1989, *ApJ*, 345, 752
- Ferrando, P. 1993, *Invited, Rapporteur and Highlight Papers*, ed. D. A. Leahy, R. B. Hicks, & D. Vankatesan (World Scientific), 23rd ICRC, Calgary
- Ferrando, P., Lal, N., McDonald, F. B., & Webber, W. R. 1991, *A&A*, 247, 163
- Fichtner, H., Neutsch, W., Fahr, H. J., & Schlickeiser, R. 1991, *ApJ*, 371, 98
- Ginzburg, V. L., & Syrovatskii, S. I. 1964, in *The Origin of Cosmic Rays* (Pergamon Press)
- Higbie, P. R., Peterson, J. D., Rockstroh, J. M., & Webber, W. R. 1999, *Proc. of the 26th ICRC*, 4, 251
- Hummel, E., Lesch, H., Wielebinski, R., & Schlickeiser, R. 1988, *A&A*, 197, L29
- Ipavich, F. M. 1975, *ApJ*, 196, 107
- Kodeira, K. 1974, *PASP*, 26, 266
- Krymsky, G. F. 1977, *Dokl. Akad. Nauk. SSSR*, 234, 1306
- Kulsrud, R. M., & Pearce, W. D. 1969, *ApJ*, 156, 445
- Leahy, D. A., & Xinji, W. 1989, *PASP*, 101, 607
- Li, Z. W. 1985, in *Proceedings of Beijing Normal University*, 4, 65
- Lukasiak, A., Ferrando, P., McDonald, F. B., & Webber, W. R. 1994, *ApJ*, 423, 426
- McKenzie, J. F., & Völk, H. J. 1982, *A&A*, 116, 191
- Neuhäuser, R., & Trümper, J. 1999, *A&A*, 343, 151
- Normandeau, M., Taylor, A. R., & Dewdney, P. E. 1996, *Nature*, 380, 687
- Ptuskin, V. S., Völk, H. J., Zirakashvili, V. N., & Breitschwerdt, D. 1997, *A&A*, 321, 434
- Seiradakis, J. H. 1976, in *The Structure and Content of the Galaxy and Galactic Gamma Rays* (NASA CP-002; Washington: Government Printing Office), 265
- Simpson, J. A., & Garcia-Muñoz, M. 1988, *SSR*, 46, 205
- Stecker, F. W., & Jones, F. C. 1977, *ApJ*, 217, 843
- Strong, A. W., Benett, K., & Bloemen, H., et al. 1996, *AAS* (3rd COMPTON Symp., München, 1995), 120, 381
- Strong, A. W., Bloemen, J. B. G. M., Dame, T. M., et al. 1988, *A&A*, 207, 1
- Strong, A. W., & Mattox, J. R. 1996, *A&A*, 308, 21
- Strong, A. W., & Moskalenko, I. V. 1998, *ApJ*, 509, 212
- Strong, A. W., Moskalenko, I. V., & Reimer, O. 2000, *ApJ*, 537, 763
- Toptygin, I. N. 1985, *Cosmic Rays in Interplanetary Magnetic Fields* (Reidel, Amsterdam)
- Tüllmann, R., Dettmar, R.-J., Soida, M., Urbanik, M., & Rossa, J. 2000, *A&A*, 364, L36
- van den Bergh, S. 1990, *AJ*, 99, 843
- van den Bergh, S. 1991, in *Supernovae*, ed. S. Woosley (Springer, New York), 711
- Völk, H. J. 2000, in *AIP Conf. Proc. 515, GeV-TeV Gamma Ray Astrophysics Workshop: Towards a Major Atmospheric Cherenkov Detector VI*, ed. B. L. Dingus, M. H. Salamon, & D. B. Kieda (New York: AIP), 281
- Wang, Q. D., Walterbos, R. A. M., Steakley, M. F., Norman, C. A., & Braun, R. 1995, *ApJ*, 439, 176
- Webber, W. R., Lee, M. A., & Gupta, M. 1992, *ApJ*, 390, 96
- Wentzel, D. G. 1974, *ARA&A*, 12, 71
- Zirakashvili, V. N., Breitschwerdt, D., Ptuskin, V. S., & Völk, H. J. 1996, *A&A*, 311, 113